

General Disclaimer

One or more of the Following Statements may affect this Document

- This document has been reproduced from the best copy furnished by the organizational source. It is being released in the interest of making available as much information as possible.
- This document may contain data, which exceeds the sheet parameters. It was furnished in this condition by the organizational source and is the best copy available.
- This document may contain tone-on-tone or color graphs, charts and/or pictures, which have been reproduced in black and white.
- This document is paginated as submitted by the original source.
- Portions of this document are not fully legible due to the historical nature of some of the material. However, it is the best reproduction available from the original submission.

Earth Models Consistent with Geophysical Data

Frank Press

Department of Earth and Planetary Sciences
Massachusetts Institute of Technology

Cambridge, Mass. U.S.A.

FACILITY FORM 608

N70-27127	
(ACCESSION NUMBER)	(THRU)
<u>38</u>	<u>1</u>
(PAGES)	(CODE)
<u>CA-109835</u>	<u>13</u>
(NASA CR OR TMX OR AD NUMBER)	

ABSTRACT

A suite of the most recently available geophysical data are inverted by an improved Monte Carlo procedure. The data are derived from surface waves for oceanic paths, eigen vibrations of the earth, elastic wave travel time and $dt/d\Delta$ data, mass and moment of inertia of the earth. A low velocity zone is required for the suboceanic mantle as is a high density lithosphere. The high density is related to eclogite fractionation from the underlying, partially molten asthenosphere in a process involving the creation and spreading of the lithosphere. If the asthenosphere is pyrolite or peridotite then an increase of mean atomic weight across the transition zone seems required. Fairborn's new $dt/d\Delta$ data for the lower mantle seem to show a higher shear velocity gradient than previously supposed. If correct, a compensatory lower density gradient is required. This may indicate a depletion of iron with depth in the lower mantle. The density at the top of the core is surprisingly well constrained to the range 9.9-10.2 gm/cc, a value appropriate for a mixture of iron and about 15 wt % silicon.

I. Introduction

A major goal of geophysics is to uniquely specify the distribution of two elastic velocities and density with depth in the earth and to relate these distributions to variations in composition, phase, and temperature in the interior. Impediments which block these achievements are many. It has not been proved in the mathematical sense that a unique solution can be obtained, although BACKUS and GILBERT (1968) have shown that under certain circumstances stable weighted averages (over depth) can be calculated. Furthermore, the data set available for recovering earth structure is incomplete and imprecise. Finally the equations of state available for interpreting elasticity and density distributions in terms of composition, state, etc. are tentative ones based on uncertain theories and assumptions and limited laboratory data.

Despite these difficulties it may be possible even with the presently available data to make some meaningful statements about the interior. In this paper we explore this possibility using the most recent and best available data in a Monte Carlo inversion procedure. Our results and conclusions supersede those presented in earlier papers (PRESS, 1968 a & b) because we are able to fit models to new, more extensive and accurate data with greater speed and better precision.

II. Method

The Monte Carlo method uses random selection to generate large numbers of models in a computer, subjecting each model to a test against geophysical data. Only those models are retained whose properties fit the data within a prescribed tolerance. The procedure offers the advantage that successful models are found without bias, preconceived ideas or uncertain assumptions of equations of state or composition. If the program is efficient so that a

very large number of models are examined, the retained models can be considered as representative of the family of successful models which fit the data. When the successful models fall in a narrow band, geophysically meaningful conclusions can often be reached despite our inability to specify a single unique model. Under certain conditions (BACKUS and GILBERT 1968) a single successful model can provide unique, local averages of density or velocity.

We have modified the Monte Carlo procedure reported last year (PRESS, 1968 a) speeding up the process by 1-2 orders of magnitude. This improved efficiency enabled us to find a larger number of successful models fitting a more extensive suite of data with better precision. The flow diagram of the currently used system (fig. 1) is printed with each run of the program and provides diagnostics so that controlling constants can be set for maximum efficiency. The figure shows the diagnostics following a run of 3347 seconds on an IBM 360-65 computer which yielded 11 successful models at a cost of about \$10 per successful model. SLMD is the random selection procedure for compressional velocity (α), shear velocity (β) and density (ρ). TTT is a test of the model against observed travel times using BULLEN'S (1961) method in which the earth is treated as a multi-layered sphere, the velocity varying according to a power law within each layer. VRPR uses a table of variational parameters (WIGGINS 1968) stored permanently in a data cell of the computer to test the perturbation of the eigenperiods due to velocity, density or core radius perturbations. This test is made after the selection of density and velocity models, the latter in order to eliminate early in the process those models which cannot be brought into agreement with eigenperiod data by density perturbations. MASMOM tests each density model against mass and moment of inertia of the earth. The flow diagram shows branching

according as the several tests are passed or failed. Each box shows the number of times the corresponding step was repeated, the average time and total time for each step and the percentage of model passing. Thus the time distribution over the various components of the program is available for adjustment of input constants for maximum efficiency and insight is provided as to how the various geophysical constraints figure in the elimination of models. A key requirement of the Monte Carlo method is that the selection procedure produce an unbiased, representative suite of models for examination. Figures 2, 3, and 4 show a run in which 25 models were generated, bypassing tests against geological data. It is seen that the velocity and density space between the permissible bounds is nearly uniformly filled. Since millions of earth models were generated and examined in this study it would be surprising if continued operation of the program would produce a successful model significantly different from those presented later in this paper. Some additional features of the program and procedures used are as follows:

1. The earth is assumed to be spherically symmetrical and isotropic, with an oceanic crust-upper mantle structure. The radius of the core is selected randomly for each model in the range 3473 ± 25 km.
2. Although α, β, γ could be varied at 88 points in the earth, we chose the time saving device of randomly varying 19 points, (see fig. 5, section D for their location) obtaining the remaining values by linear interpolations.
3. The fluid core was assumed to be adiabatic. The density selection procedure for the mantle below 1000 km eliminated models with extreme density gradients. The gradients in α, β, γ were restricted to a maximum number of reversals in sign (typically 2 or 4) to restrict the complexity of models.
4. The rigidity for the inner core only affects the mode S_2^o . Although zero rigidity was assumed in this paper, the

systematic, negative residuals for ${}_0S_2$ found in our models will be used to infer a rigidity for the inner core.

5. Several exact calculations of eigenperiods were made to check the accuracy of the variational parameter method. The differences were small and well within the uncertainty of the data.

III. The Data

Successful models were required to fit the following data:

1. Earth mass, $M=5.976 \times 10^{27}$ grams; dimensionless moment of inertia $I/Ma^2 = .3308$

2. Compressional velocity distribution in the mantle fixed very close to the models determined by JOHNSON (1969) and FAIRBORN (1969), based on $dt/d\Delta$ analyses of array data. P and Pcp travel times fit the latest data (HERRIN et al. 1968) to ± 1 sec. The compressional velocity distribution in the core was fixed to the recent model of HUSEBYE and TOKSOZ (1969).

3. Shear velocities below 800 km were restricted to lie within the narrow bounds reported by FAIRBORN (1969) who used Monte Carlo methods to interpret travel time and $dt/d\Delta$ data obtained from the Large Aperture Seismic Array (LASA). Wider bounds were used above 800 km. Travel times of S and ScS were required to fit FAIRBORN'S data to within ± 5 sec at 10 distances between 25° and 100° and a single failure was sufficient to reject a model. These travel time data primarily constrain the mantle below 800 km.

4. Eigenperiods tested were ${}_0S_0$, ${}_0S_2$ through ${}_0S_{22}$, ${}_1S_2$, ${}_1S_3$, ${}_1S_5$, ${}_1S_6$, ${}_1S_8$, ${}_1S_{12}$, ${}_2S_4$, ${}_2S_6$, ${}_2S_{10}$; toroidal oscillations tested were ${}_0T_3$ - ${}_0T_{21}$, ${}_cT_2$ not being used because of its uncertain value; models were also required to fit surface wave phase velocities for predominantly oceanic paths as follows: Rayleigh waves in the period range 125-325 seconds (BEN-MENAHEM, 1965); Love waves in the period range 80-340 seconds (TOKSOZ and ANDERSON, 1966). We used the eigenperiod data as reviewed and summarized by DERR (1969)

except as follows: S_2^o - 3229.0 seconds, S_{11}^o - 537.5 seconds. The uncertainty in the eigenperiod and dispersion data was taken to be $\pm 0.4\%$ due to asphericity, rotational splitting and experimental errors (DAHLEN 1968). An error analysis of the oceanic surface wave data indicates than an accuracy better than 1% was achieved. Comparison with phase velocities for other oceanic paths verified this for Love and Rayleigh waves. The fit of S_o was required to be within $\pm 0.1\%$. Actually the final models fit most of the data to about half these tolerances. Figure 5 shows the computed eigenperiods and the residuals for a typical model.

IV. Results

The results reported here supersede our earlier conclusions (PRESS 1968) because of the new and more extensive data set inverted in this paper. The effects of lateral variation were reduced by deriving higher mode data from oceanic surface wave phase velocities. Moreover the new procedure enabled us to find a much larger number of successful models and therefore a more representative selection from the set of successful models.

The shear velocity and density distribution are plotted in figs. 6, 7, and 8 and are also tabulated (together with the fixed compressional velocity distribution) in figs. 9-13.

V. The Upper Mantle Under Oceans

Without exception every successful model contains a low velocity zone for shear waves which centers at depths between 150 and 250 km. If the lid of this zone is characterized by $\beta > 4.5 \text{ km/sec}$, then its thickness is 50-100 km. We failed to find a single model without a low velocity zone despite a special search in which 162,000 monotonic shear velocity models were examined. A low velocity zone seems required by our data since essentially every possible model without it was examined and eliminated. Nevertheless, HADDON and BULLEN (1969) reported a successful monotonic model, probably because: (1) they only use modes through $n=44$, whereas our data go to $n=105$; (2) our Love wave phase velocities trend towards lower values than the HB data (see fig. 14).

The several mechanisms which might account for the low velocity

partial (grain boundary) melting for the following reasons: (1) shear velocity and Q are sensitive to the presence of small amounts of melt along grain boundaries; (2) data presented at this conference by several investigators show that the temperature at which melting begins in the wet state for candidate upper mantle mineral assemblages is sufficiently low to be reached by the geotherm for most thermal models of the earth; (3) the partial melting product of candidate mineral assemblages can account for basaltic vulcanism; (4) a partially molten, low strength zone would serve to mechanically decouple the lithosphere from the underlying mantle as is required by some proposed mechanisms for the spreading sea floor.

The density values shown in figs. 7 and 15 fill the entire permissible range at the M-discontinuity indicating a lack of constraint by the geophysical data. However, the initial density gradients are all positive and in the vicinity of 100 km all the values fall in the narrow band $3.5\text{-}3.6 \text{ gm/cm}^3$ in the upper part of the permissible range. As a check on this result a special search was made without success to find models with densities below 3.4 gm/cm^3 in this depth range. For additional confirmation of this result we applied the BACKUS and GILBERT (1968) δ -ness criterion using weighting functions computed for our data by WIGGINS (1969). According to Backus and Gilbert, if the weighting functions are concentrated over narrow depth intervals, a stable local average can be obtained from a single model. Using this procedure every one of the models yielded an average density in the range $3.5\text{-}3.6 \text{ g/cm}^3$ for the depth interval 75-125 km. Presumably the average density near 100 km is uniquely determined in the sense that any model computed from our data set should give the same value.

Unfortunately the density resolution deteriorates below 100 km as can be seen by the wider band of Monte Carlo solutions. At

300 km the resolving length inferred from the δ -ness criterion is 200 km. One might argue on physical grounds that the lower density solutions should be favored below 150 km because of the low shear velocities. This implies a density reversal from the lithosphere to the asthenosphere ($3.5-3.6 \text{ gm/cm}^3$ at 100 km to $3.3-3.5 \text{ gm/cm}^3$ at 300 km).

More complex models were found involving two low velocity or two low density zones in the upper mantle. However, these models yield the same indication of high density near 100 km.

The indicated density for the lithosphere near 100 km is so high as to narrow the range of its possible composition to an eclogitic facies. This follows if the selection is made from the current petrologic hypotheses for the constitution of the upper mantle. In fig. 15 densities computed by CLARK and RINGWOOD (1964) for a mantle composed of pyrolite (peridotite or dunite would give about the same values) and eclogite. Only the eclogite model is consistent with our results between 80 and 150 km. Either model is acceptable above this region and the pyrolite model is weakly favored near 300 km. A more extended discussion of these results can be found in another paper (PRESS 1969) where a hypothesis is proposed in which eclogite fractionation from the underlying, partially molten asthenosphere is involved in the creation and spreading of the sub-oceanic, rigid, lithospheric plate. BIRCH (1969) also interpreted these results to imply an eclogitic composition.

VI. The Transition Zone

Seismic array data have been used recently to establish rapid velocity changes near 400 and 700 km (see for example JOHNSON, 1967). These results have been incorporated in our models by fixing the compressional velocity and narrowing the range of permissible shear velocities at these depths to conform to the rapid increases, as seen in fig. 6. Although no such restrictions were placed on

the density values the rapid increase in density across the transition zone is evident on all models in fig. 7. This increase is due to compression, and to phase changes and possibly to composition changes. Phase transitions are ^{also} inferred from the laboratory verification of the olivine-spinel phase change at pressures corresponding to depths near 400 km and by the theoretical and experimental indications for a post-spinel phase transformation. (See for example, D.L. ANDERSON (1967) or H. FUJISAWA (1968)).

The occurrence of composition changes in the transition zone are more difficult to establish. BIRCH (1961) used the velocity change $\Delta\alpha$, and the density change $\Delta\rho$ to separately estimate the effects of phase and composition change. Using $\Delta\alpha$ and $\Delta\rho$ values for each model between 333 and 871 km, allowing .36 gm/cc for compression and using Birch's values for $(\partial\alpha/\partial\rho)_m$, $(\partial\rho/\partial_m)_{T,p}$, $(\partial\alpha/\partial_m)_\rho$, the change in mean atomic weight Δm was computed across the transition zone for each model. Those models with reduced densities in the asthenosphere ($\rho < 3.4$ gm/cc) showed an increase of 1-2 units in m . Thus for an asthenosphere with $m \sim 21$, and $Fe/Fe + Mg \sim 0.1$, as would be the case for peridotite or pyrolyte, the $Fe/Fe + Mg$ ratio would increase to 0.2 or 0.3 across the transition zone. On the other hand, no increase in m was found for those models with a high density asthenosphere ($\rho > 3.5$ gm/cc). If the entire upper mantle is closer to eclogite in its iron content no increase in the $Fe/Fe + Mg$ ratio seems to be required across the transition zone. In a recent paper D.L. ANDERSON (1968) proposed that $\Delta m \sim 1.5$ and BIRCH (1961) gave $\Delta m \sim 1.0$ for one model.

VII. The Lower Mantle

Our results for the lower mantle rest heavily on Fairborn's independent determinations of a band of shear velocity distributions consistent with $dt/d\Delta$ and travel time data obtained at LASA. The range of shear velocities permitted by Fairborn's results is quite

narrow, as can be seen in fig. 6. This enables us to use eigen-period data to constrain the density in the lower mantle to a greater degree than was possible before. Fairborn's shear velocity envelope shows a higher gradient than has usually been assumed (e.g. when compared to the Gutenberg model) and this requires a compensatory reduction in the density gradient in order to fit the spheroidal eigenperiod data. The results are shown in figs. 6 and 7. The density is constrained surprisingly well, to within about 0.2 gm/cc for most of the lower mantle. The density gradient is less than the adiabatic gradient as can be seen by comparison with the lower bound which approximates an adiabatic gradient. Figure 16 shows our band of solutions plotted against D.L. ANDERSON'S (1968) theoretical calculations for density of the solid solution series forsterite-fayalite and his summary of shock wave data. The band of density solutions is discordant with respect to profiles of constant composition, suggesting a change of mean atomic weight from 22-23 at the top of the lower mantle to 20-22 at the bottom of the mantle. This implies a depletion of iron with depth with the Fe/Fe + Mg ratio going from 0.2-0.3 to 0.1-0.2. Although superadiabatic temperature gradients might also account for the smaller density gradient, the augmented shear velocity gradient argues against this.

This can also be seen in figure 17 where the bulk sound velocity and density values for each model are plotted. The figure also shows the shock wave values for Twin Sisters dunite ($m=20.9$) and hortonolite dunite ($m=25.1$), as reduced by AHRENS, ANDERSON and RINGWOOD (1969). Although the data are scanty, a reduction in mean atomic weight from 22-23 at 871 km to 20-21 at 2898 km is indicated. The discordance with lines of constant composition seems too large to be accounted for by superadiabatic temperature gradients. WANG (1969) also suggested that these data might indicate decreasing m in the lower mantle. If subsequent studies do not establish Fairborn's shear velocity distribution as a world wide phenomenon, this conclusion will

have to be changed.

VIII. The Mantle

The $c-\rho$ graph illustrates the main features of the mantle discussed earlier. The olivine-spinel phase transformation is evidenced between 371 km and 421 km by models with increasing c and ρ . Between 421 km and 621 km models with large increases in ρ and with little change in c could be interpreted as the result of compression and increasing iron content, the two effects having the same sign for ρ and opposite signs for c . The increase in c and ρ between 621 km and 721 km implies a phase change as the major feature. Decomposition of the ferro-magnesium-alumininum silicate to close packed simple oxides, or transformations to structures such as ilmenite or perovskite have been suggested for this region (BIRCH 1952, D.L. ANDERSON 1967, RINGWOOD 1969).

The distributions for ϕ and k/μ in the mantle are given in figs. 18 and 19.

XI. The Core

Results for the core are shown in figs. 8 and 20. The assumption of adiabaticity in the fluid core and the constraints imposed by the data prescribe the densities to the surprisingly small range of .25 gm/cc. The δ -ness criterion also indicates high resolving power for density at the top of the core. Using the shock wave data of McQUEEN and MARSH (1966) and BALCHAN and COWAN (1966) we see that iron alloyed with a miscible, abundant element such as silicon (15 wt %) would account for the core densities. There is no control on the density in the inner core with the data used here. Changes in the core radius ranged from -3 km to + 10 km.

The requirement for finite rigidity of the inner core was evidenced in an interesting way. Our procedure neglects core

rigidity and the only mode affected by this assumption, σS_2 showed negative residuals for every model. Using ALSOP'S (1963) correction for rigidity resulted in a reduction of the residuals, for σS_2 , the largest discrepancy being .15%. This agrees with D.L. ANDERSON'S conclusions concerning rigidity in the inner core (1969).

X. Discussion

The question of uniqueness arises in all discussions of internal earth structure. The Backus-Gilbert δ -ness criterion demonstrates how stable local averages can be computed for α , β and ρ using eigenperiod data. However with currently available data the resolving power is adequate at too few places in the earth. Also the procedure does not yet allow for travel time or $dt/d\Delta$ data which under certain circumstances have high resolving power, nor does it consider errors in data. The band of solutions provided by the Monte Carlo method, if sufficiently narrow and if derived without bias from a large and representative selection of models, can under certain circumstances lead to meaningful conclusions. Unfortunately one is never quite sure that continued search would not reveal models significantly different from those already found, vitiating the conclusions. The use of physical arguments, laboratory experiments, theoretical-empirical equations of state will eventually provide powerful constraints. However the poor state of knowledge of the behavior of materials at internal earth pressures and temperatures, though improving rapidly, is a severe, current limitation.

With regard to the present paper and the other studies cited, we believe the following results are firm if the assumptions and data are correct:

1. The low velocity zone for shear waves in the sub-oceanic upper mantle. The parameterization included sufficiently few elements so that all possible models without a low velocity zone

'could be tested and eliminated.

2. The high density for the lithosphere near 100 km. The δ -ness criterion has high resolving power for density at this depth and the narrow spread of Monte Carlo solutions indicate that errors in surface wave data of about 10% do not weaken the constraint. As mentioned earlier, we believe this accuracy was achieved.

3. The rapid velocity increase near 400 km and its association with the olivine-spinel transformation: directly obtainable from $dt/d\Delta$ data (with minor depth uncertainty); the phase transformation was experimentally verified in the laboratory and olivine is almost certainly a major constituent of the upper mantle.

4. The rapid velocity increase near 700 km: directly obtainable from $dt/d\Delta$ data (with some depth uncertainty).

5. The density at the top of the core is between 9.9 and 10.2 gm/cc. The δ -ness criterion shows high resolving power and the spread of Monte Carlo solutions is small.

XI. Acknowledgements

Joel Karnofsky was an invaluable research assistant in this project. R.A. Wiggins kindly made his δ -ness weighting functions available in advance of publication. D.L. Anderson, F. Birch, C. Wang, J. Fairborn, K.E. Bullen, J.Derr, M.N. Toksöz , made manuscripts available in advance of publication. A grant from the Australian National University made it possible for me to participate in this Symposium. The technique was developed as part of an inversion procedure for lunar data with support from the National Aeronautics and Space Administration under grant NGR 22-009-123. The application to the earth was supported by the Advanced Projects Research Agency and monitored by the Air Force Office of Scientific Research under contract AF 49(638) -1632.

Figures

Figure 1 - Flow diagram of Monte Carlo program during a run in which 531, 881 density models and 5025 shear velocity models were tested and yielded 11 successful models.

Figure 2 - Twenty-five shear velocity models of the mantle not subjected to geophysical constraints to test distribution of randomly generated models.

Figure 3 - Unconstrained mantle densities (see Figure 2 caption).

Figure 4 - Unconstrained core densities (see Figure 2 caption).

Figure 5 - Results for a typical model. Section A line 1: mass and moment of inertia; lines 2-4: p, Δ , theoretical times, model times and residuals for S and ScS. Section B: model eigenperiods and residuals against observed eigenperiods. Section C: model printout. Section D: depths at which parameters were varied and corresponding Δ values.

Figure 6 - Twenty-seven successful shear velocity models for the mantle. Ticks on upper and lower bounds show where parameter was randomly varied.

Figure 7 - Density in the mantle (see Figure 6 caption).

Figure 8 - Density in the core (see Figure 6 caption).

Figure 9 - Tabulated parameters of successful models. Change in core radius shown in lower right corner. Each model has fixed crustal layers for depth, alpha, beta and rho as follows:
0., 1.52, 0. 1.03; 3., 6.55, 3.73, 2.84; 10, 6.55, 3.73, 2.84.

Figure 10 - See Figure 9

Figure 11 - See Figure 9

Figure 12 - See Figure 9

Figure 13 - See Figure 9.

Figure 14 - Differences in Love wave phase velocity data used by Hadden and Bullen and by Press which accounts for latter's requirement of low velocity zone. Points show how models fit the data.

Figure 15 - Successful density models for the upper mantle plotted together with Clark and Ringwood models for pyrolite and eclogite.

Figure 16 - D. L. Anderson's theoretical models and his summary of experimental data plotted with our density solutions shown by the shaded band.

Figure 17 - Bulk sound velocity-density plot for successful models of the mantle together with static and shock wave data for dunite and forsterite-fayalite.

Figure 18 - Seismic parameter ϕ for the mantle obtained from successful models.

Figure 19 - Ratio K/μ for the mantle obtained from successful models.

Figure 20 - Band of core densities from successful models together with shock wave density data for Fe, Ni and Fe+ 19.8 wt.% Si.

REFERENCES

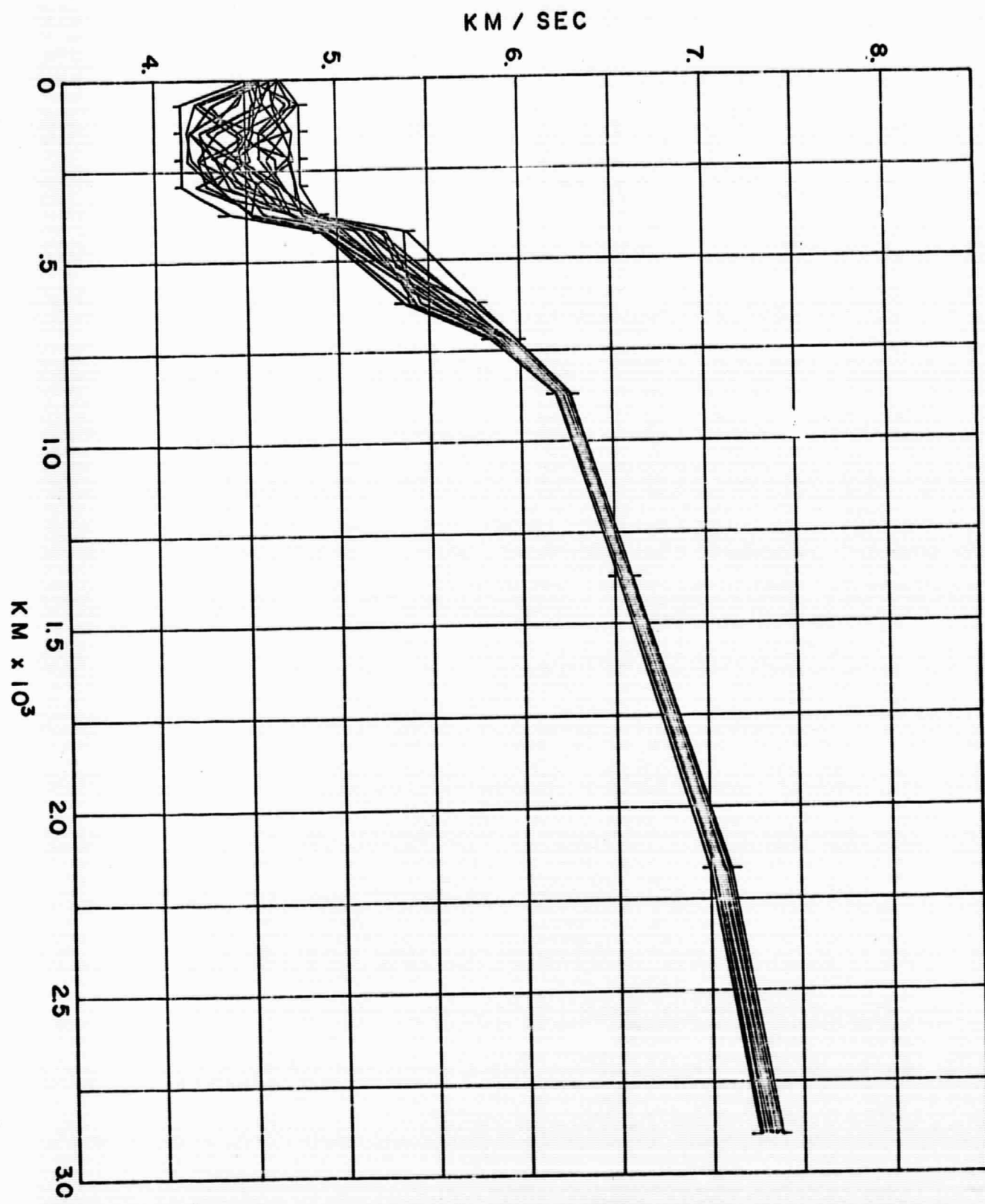
- AHRENS, T. J., D. L. ANDERSON and A. E. RINGWOOD (1969), in press.
- ALSOP, L. E. (1963), Bull. Seismol. Soc. Am., 53, 503.
- ANDERSON, D. L. (1967), Science, 157, 1165.
- ANDERSON, D. L. (1968), Earth and Planet. Sci. Let., 5, 89.
- ANDERSON, D. L. (1969), this volume.
- BACKUS, G., and F. GILBERT (1968), Geophys. J., 16, 169.
- BALCHAN, A. S., and G. R. COWAN (1966), J. Geophys. Res., 71, 3577.
- BEN-MENAHEM, A. (1965), J. Geophys. Res., 70, 4641.
- BIRCH, F. (1952), J. Geophys. Res., 57, 227.
- BIRCH, F. (1961), Geophys. J., 4, 295.
- BIRCH, F. (1969), this volume.
- BULLEN, K. E. (1961), Geophys. J., 4, 93.
- CLARK, S. P., and A. E. RINGWOOD (1964), Rev. Geophys., 2, 35.
- DAHLEN, F. A. (1968), Geophys. J., 16, 329.
- DERR, J. (1969), in press, Bull. Seismol. Soc. Am.
- FAIRBORN, J. W. (1969), in press, Bull. Seismol. Soc. Am.
- FUJISAWA, H. (1968), J. Geophys. Res., 73, 3281.
- HADDON, R. A. W. and K. E. BULLEN (1969), in press.
- HERRIN, E., W. TUCKER, J. TAGGART, D. W. GORDON, and J. L. LOBDELL (1968), Bull. Seismol. Soc. Am., 58, 1273.
- HUSEBYE, E. S. and M. N. TOKIOZ (1969), in press, J. Geophys. Res.
- JOHNSON, L. R. (1967), J. Geophys. Res., 72, 6309.
- JOHNSON, L. R. (1969), in press.

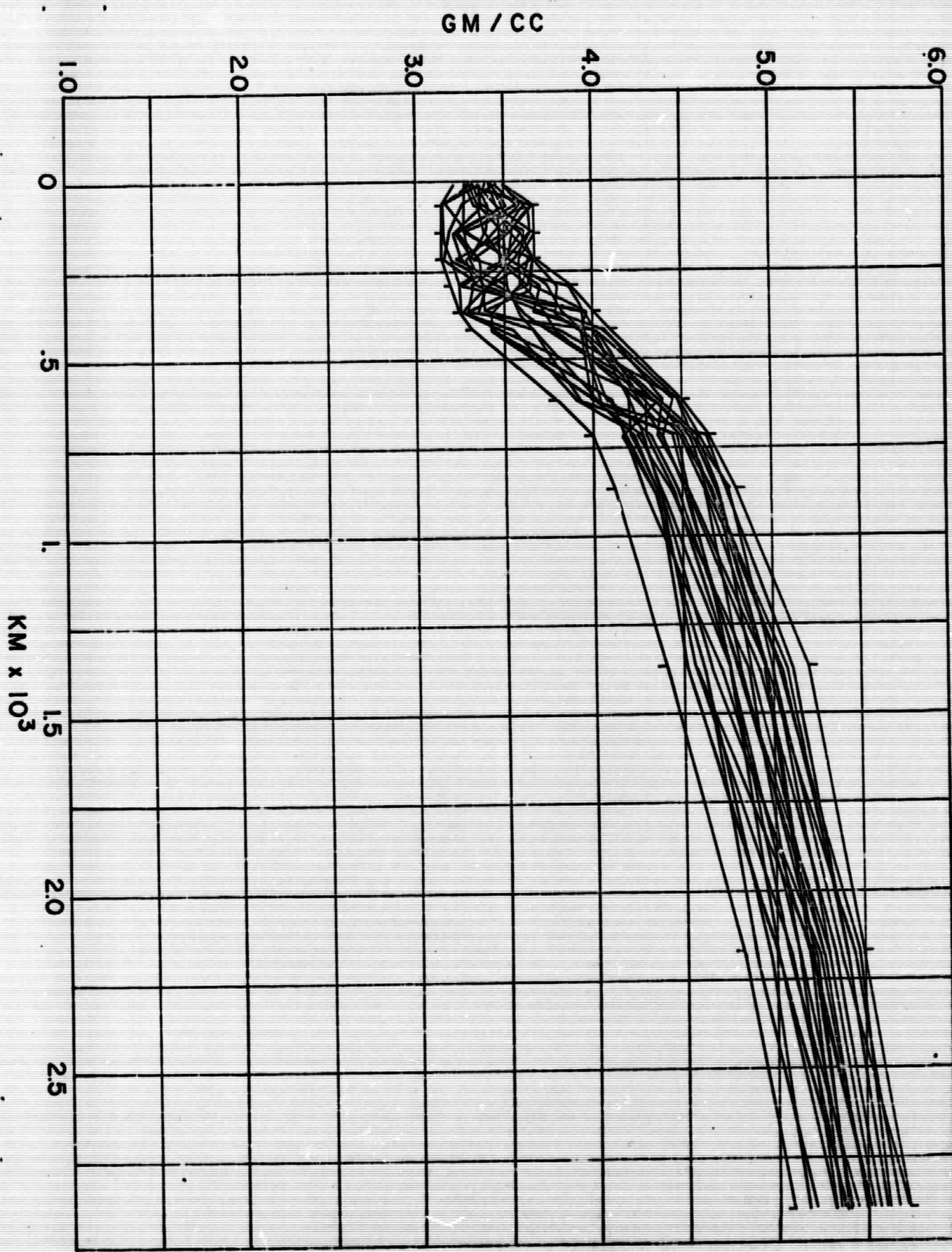
- McQUEEN, R. G. and S. P. MARSH (1966), J. Geophys. Res., 71, 1751.
- PRESS, F. (1968a), J. Geophys. Res., 73, 5223.
- PRESS, F. (1968b), Science, 160, 1218.
- PRESS, F. (1969), in press, Science.
- RINGWOOD, A. E. (1969), this volume.
- TOKSOZ, M. N. and D. L. ANDERSON (1966), J. Geophys. Res., 71, 1649.
- WANG, C. (1969), in press, J. Geophys. Res.
- WIGGINS, R. A. (1968), Phys. Earth Planetary Interiors, 1, 201.
- WIGGINS, R. A. (1969), in preparation.

DIAGNOSTIC NUMBER 18
TIME SINCE LAST DIAGNOSTIC 191.61 SECONDS
TOTAL COMPUTATION TIME 3347.42 SECONDS

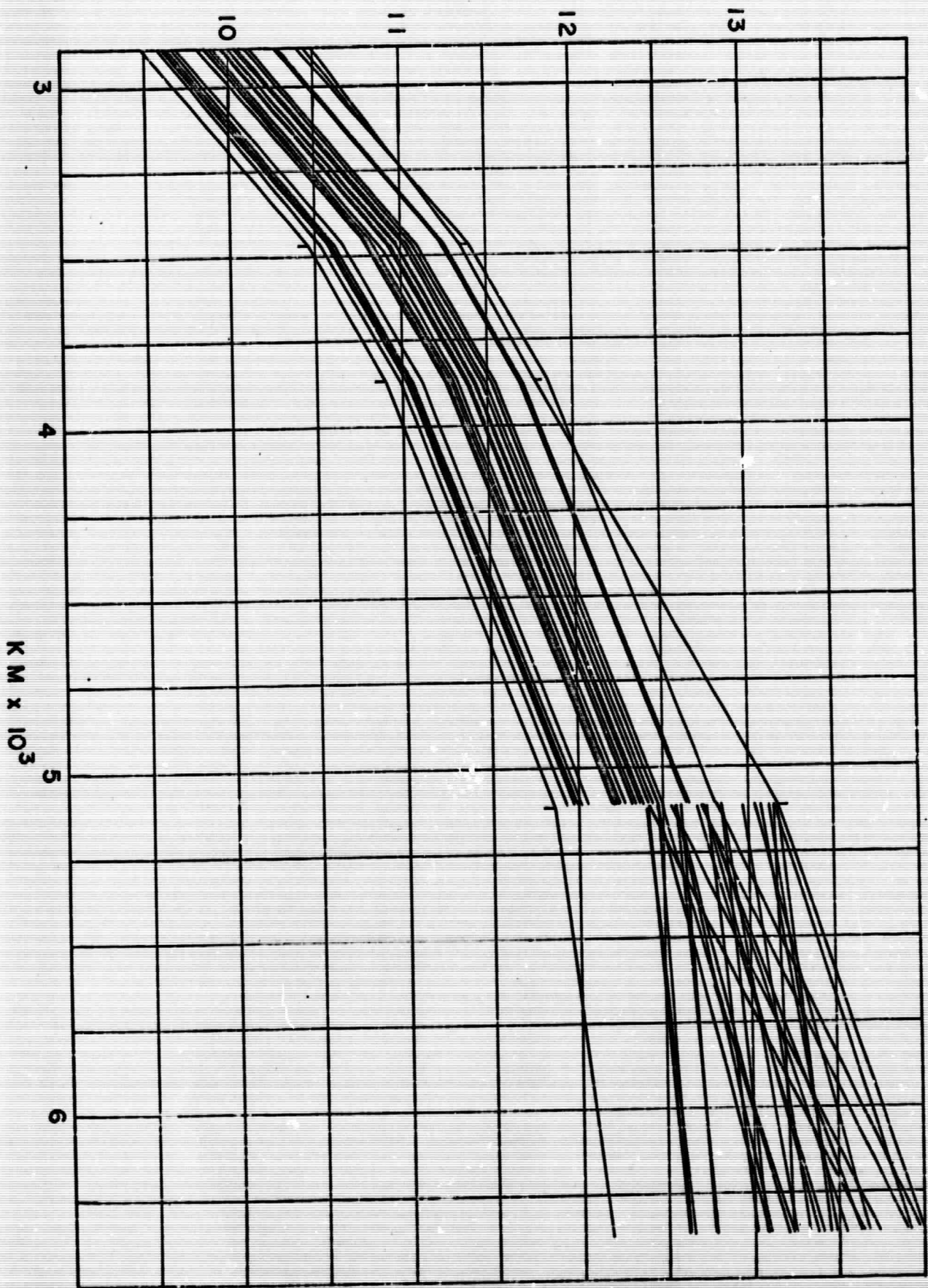
ALPHA SLMD	BETA SLMD	RHO SLTMD	VPRR
COUNT = 450	COUNT = 5025	COUNT = 365916	COUNT = 365916
AV TIME = 0.00140	AV TIME = 0.00192	AV TIME = 0.00085	AV TIME = 0.00085
TO TIME = 0.63	TO TIME = 9.65	TO TIME = 310.52	TO TIME = 310.52
NUMB PASS = 11	% PASSING = 8.53	A 6 MODELS - 125	A 6 MODELS - 125
% LUMPS TILL SUK	1- 300 1	1- 300 1	1- 300 1
401- 600 0	401- 600 0	401- 600 0	401- 600 0
601- 900 4	601- 900 4	601- 900 4	601- 900 4
901-1200 2	901-1200 2	901-1200 2	901-1200 2
1201-1500 2	1201-1500 2	1201-1500 2	1201-1500 2
1501-1800 1	1501-1800 1	1501-1800 1	1501-1800 1
1801-2100 0	1801-2100 0	1801-2100 0	1801-2100 0
2101-2400 1	2101-2400 1	2101-2400 1	2101-2400 1
2401-2700 0	2401-2700 0	2401-2700 0	2401-2700 0
2701-3000 0	2701-3000 0	2701-3000 0	2701-3000 0
FAILED 118	FAILED 118	FAILED 118	FAILED 118
ALPHA VTR	BETA VTR	MASHM	
% PASSING = 0.0	% PASSING = 26.25	% PASSING = 68.79	
AV TIME = 0.0	AV TIME = 0.01588	AV TIME = 0.00121	
TO TIME = 0.0	TO TIME = 79.79	TO TIME = 642.28	
ALPHA VRPR	BETA VRPR	MASHM	
% PASSING = 0.0	% PASSING = 9.78	% PASSING = 68.79	
AV TIME = 0.0	AV TIME = 0.00667	AV TIME = 0.00121	
TO TIME = 7.46	TO TIME = 8.80	TO TIME = 642.28	

THE PROGRAM STARTS AGAIN WITH A NEW CORE AFTER 150 ALPHA ITT FAILURES, OR 10 BETA ITT FAILURES, OR 3000 RHO VRPM FAILURES.





GM / CC



MODEL	1	MASS = 5.97600	I = 8.02400	1/MAR = 0.33080	M.C.D. = 11.1859	IC/MAC = 0.38854	
0.0	0.0	937.70	935.80	1.90	16.6	24.22	579.83
14.4	47.02	931.97	926.75	5.22	13.3	55.22	575.59
11.1	72.63	1260.32	1256.00	4.32	10.0	83.69	4.23
7.3	68.09	1264.38	1260.27	4.11	10.0	83.69	1375.71
0.5	2	3221.5 -7.5	4 1543.4 -3.6	6 963.7 -0.2	14 449.3 0.9	30 261.8 -0.7	50 178.7 0.5
3	2129.6 -4.6	5 1189.4 0.4	7 813.0 1.3	8 709.2 1.6	9 635.7 1.7	10 581.4 1.4	70 134.0 -0.2
12	504.2 2.2	13 474.7 1.6	15 427.0 0.8	16 407.3 0.8	17 389.8 0.4	18 374.1 0.7	11 538.9 1.4
21	335.4 -0.4	22 324.7 0.7	24 305.7 -0.0	26 289.2 -0.2	28 274.7 -0.3	32 250.2 -0.6	20 347.1 -0.3
36	229.9 -0.1	39 216.8 0.1	42 205.0 0.3	45 194.4 0.5	55 165.2 0.6	60 153.5 0.4	34 239.6 -0.4
0.1	75 125.8 -0.5	19 360.0 -0.6	11 575.9 0.2	40 201.1 -0.2	80 106.5 0.0	17 409.8 1.5	12 538.5 0.5
5	1308.4 4.4	8 738.2 1.2	11 780.3 2.4	9 673.2 1.2	10 620.1 0.7	15 452.3 -0.0	12 538.9 1.4
13	1079.3 3.3	6 928.5 3.1	14 477.3 0.3	2 2630.3 -0.7	18 391.7 1.5	19 375.2 0.7	20 360.1 -0.5
13	505.7 1.0	14 477.3 0.3	16 429.9 0.3	23 321.6 0.1	27 281.7 0.1	30 257.8 -0.1	35 225.9 -0.3
21	346.2 -0.9	22 333.4 -0.9	23 321.6 0.1	25 300.3 0.1	27 281.7 0.1	30 257.8 -0.1	35 225.9 -0.3
45	181.1 -0.7	50 164.7 -0.2	60 139.4 -0.1	70 120.8 -0.0	90 95.2 0.0	105 82.1 0.0	
0.8	1 1226.7 -0.9	3 1067.4 3.4 *	5 734.2 5.5	6 662.2 2.2	8 559.3 3.9 *	12 393.4 -3.4	
1.5	2 1473.5 1.5						
1.8	2 921.8 16.3 *	4 730.7 5.8	6 595.9 1.3	10 415.9 0.7			
2.5	* 2						
2.7							
2.8							
1	6371.0	1.52	0.0	1.03	2 6368.0	1.52	0.0
5	6361.0	8.00	4.62	3.44	6 6338.0	8.06	4.58
9	6300.0	8.16	4.50	3.56	10 6275.0	8.03	4.45
13	6200.0	8.00	4.36	3.59	14 6175.0	8.23	4.35
17	6100.0	8.54	4.38	3.55	18 6075.0	8.58	4.40
21	6000.0	8.68	4.71	3.53	22 5975.0	9.17	5.01
25	5900.0	9.75	5.37	5.57	26 5875.0	9.79	5.41
29	5800.0	9.92	5.50	3.93	30 5775.0	9.96	5.53
33	5700.0	10.48	5.77	4.29	34 5675.0	10.73	5.87
37	5600.0	11.05	6.06	4.50	38 5550.0	11.13	6.15
41	5300.0	11.53	6.37	4.62	42 5200.0	11.70	6.44
45	4800.0	12.27	6.69	4.79	46 4600.0	12.52	6.81
49	4300.0	13.23	7.12	5.12	50 3800.0	13.44	7.19
53	3600.0	13.64	7.25	5.32	54 3575.0	13.67	7.26
57	3500.0	13.75	7.28	5.37	58 3476.7	13.77	7.29
61	3425.0	8.05	0.0	10.16	62 3400.0	8.10	0.0
65	3100.0	8.64	0.0	10.69	66 2900.0	9.00	0.0
69	2300.0	9.69	0.0	11.60	70 2100.0	9.78	0.0
73	1700.0	9.95	0.0	12.03	74 1600.0	10.00	0.0
77	1400.0	10.09	0.0	12.25	78 1350.0	10.11	0.0
81	1253.0	11.15	0.0	12.88	82 1100.0	11.15	0.0
85	500.0	11.17	0.0	13.24	86 300.0	11.18	0.0
4	ALPHA REVERSALS BEFORE LAYERS	10	13	59	63		
2	BETA REVERSALS BEFORE LAYERS	6	19				
2	RHO REVERSALS BEFORE LAYERS	22	24				
5	10	22.6	23	421.0	19.3	58	2898.0
9	71	22.6	31	621.0	23.0	59	2998.0
12	146.	23.9	35	721.0	23.3	66	3471.0
15	221.	21.3	39	871.0	23.6	68	3871.0
18	296.	21.3	44	1371.0	23.2	80	5118.0
21	371.	21.4	48	2171.0	23.4	81	5118.0

D

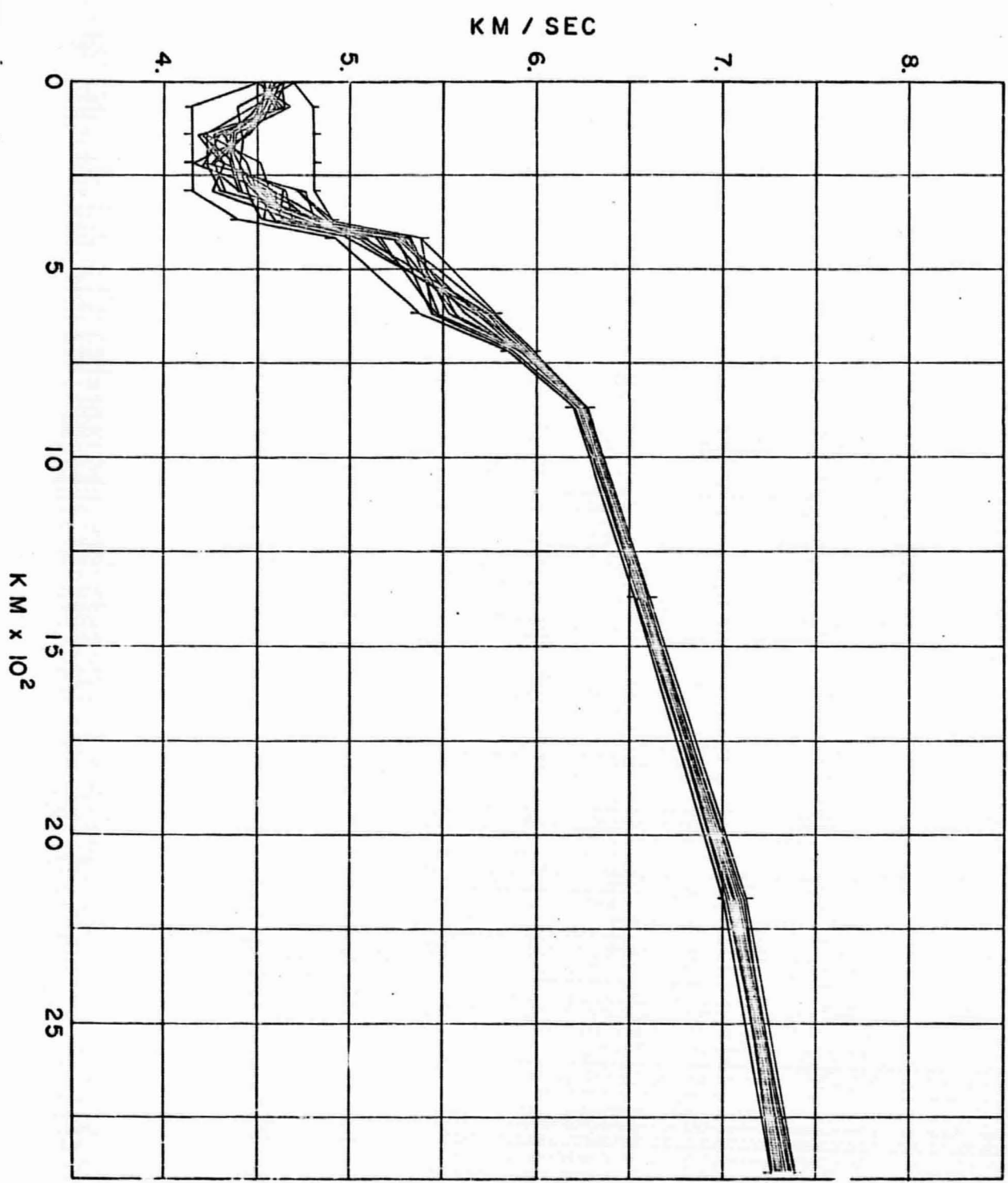
C

B

1/MAR = 0.33080	M.C.D. = 11.1859	IC/MAC = 0.38854	1.5	32.49	713.51	709.28	4.23
16.6	24.22	579.83	1.2	65.22	1173.89	1168.21	5.68
13.3	55.22	1045.72	1.0	4.21	1374.27	1.4	3.89
10.0	83.69	1039.71	0.8	94.14	1474.78	1470.89	
10.0	83.69	1375.71	1.44				
12	6225.0	6050.0	4.41	3.60	6025.0	8.65	4.36
11	6215.0	6150.0	4.47	4.34	6125.0	8.51	4.36
10	6205.0	6050.0	4.51	3.55	6025.0	8.65	4.61
9	6195.0	5950.0	4.67	3.31	5925.0	9.71	5.34
8	6185.0	5850.0	4.71	3.75	5825.0	9.88	3.84
7	6175.0	5750.0	4.76	3.75	5725.0	10.24	5.67
6	6165.0	5650.0	4.81	3.75	5625.0	11.01	6.02
5	6155.0	5550.0	4.86	4.55	5400.0	11.37	6.30
4	6145.0	5450.0	4.91	4.55	5000.0	12.02	6.57
3	6135.0	5350.0	4.96	4.95	4800.0	13.03	5.03
2	6125.0	5250.0	5.01	4.95	4600.0	12.78	6.94
1	6115.0	5150.0	5.06	4.95	4400.0	12.02	7.06
0	6105.0	5050.0	5.11	4.95	4200.0	13.03	5.03
-1	6095.0	4950.0	5.16	4.95	4000.0	11.37	6.58
-2	6085.0	4850.0	5.21	4.95	3800.0	11.37	6.30
-3	6075.0	4750.0	5.26	4.95	3600.0	11.37	6.30
-4	6065.0	4650.0	5.31	4.95	3400.0	11.37	6.30
-5	6055.0	4550.0	5.36	4.95	3200.0	11.37	6.30
-6	6045.0	4450.0	5.41	4.95	3000.0	11.37	6.30
-7	6035.0	4350.0	5.46	4.95	2800.0	11.37	6.30
-8	6025.0	4250.0	5.51	4.95	2600.0	11.37	6.30
-9	6015.0	4150.0	5.56	4.95	2400.0	11.37	6.30
-10	6005.0	4050.0	5.61	4.95	2200.0	11.37	6.30
-11	5995.0	3950.0	5.66	4.95	2000.0	11.37	6.30
-12	5985.0	3850.0	5.71	4.95	1800.0	11.37	6.30
-13	5975.0	3750.0	5.76	4.95	1600.0	11.37	6.30
-14	5965.0	3650.0	5.81	4.95	1400.0	11.37	6.30
-15	5955.0	3550.0	5.86	4.95	1200.0	11.37	6.30
-16	5945.0	3450.0	5.91	4.95	1000.0	11.37	6.30
-17	5935.0	3350.0	5.96	4.95	800.0	11.37	6.30
-18	5925.0	3250.0	6.01	4.95	600.0	11.37	6.30
-19	5915.0	3150.0	6.06	4.95	400.0	11.37	6.30
-20	5905.0	3050.0	6.11	4.95	200.0	11.37	6.30
-21	5895.0	2950.0	6.16	4.95	0.0	11.37	6.30

A

B



GM / CC

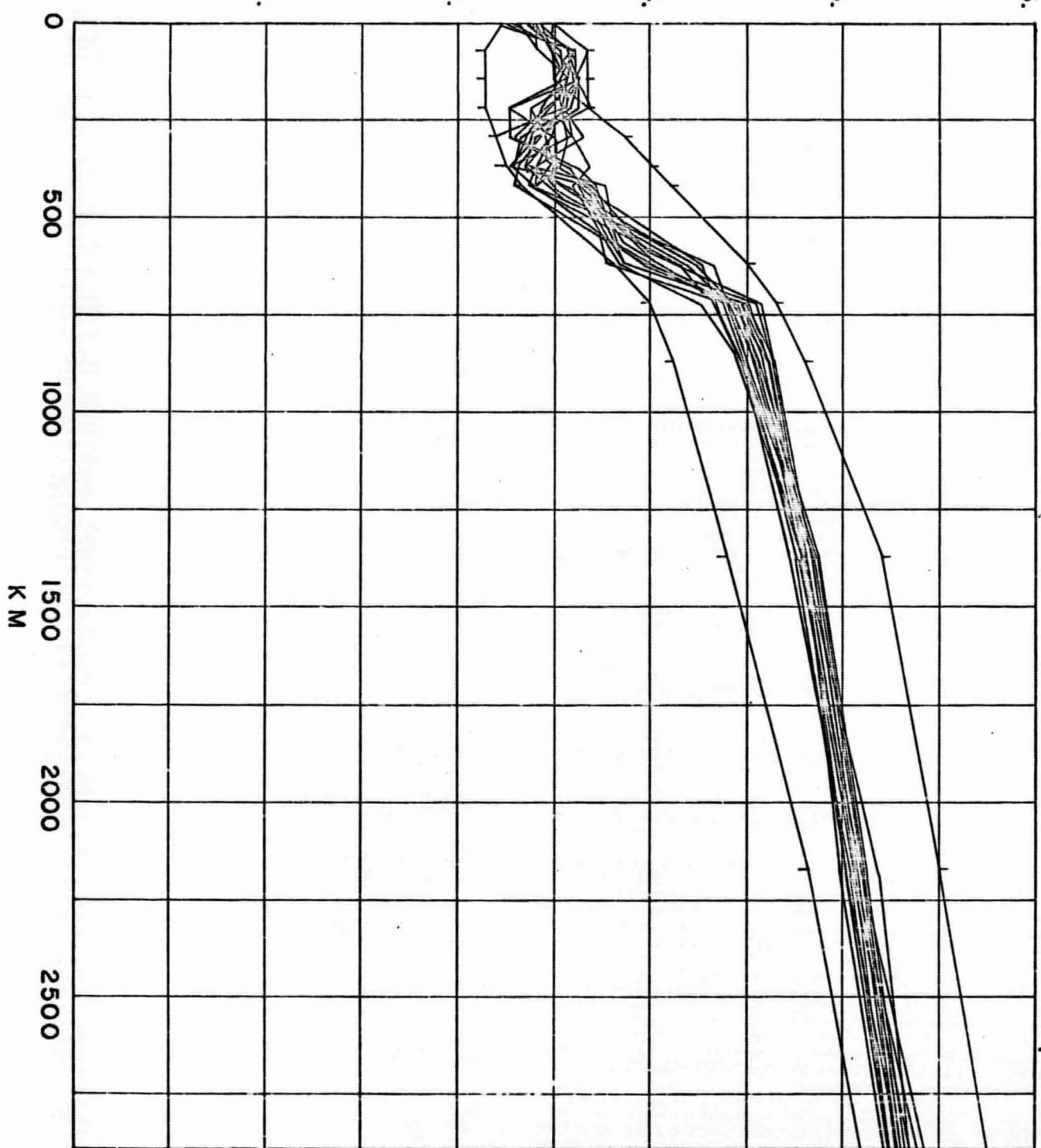
2.

3.

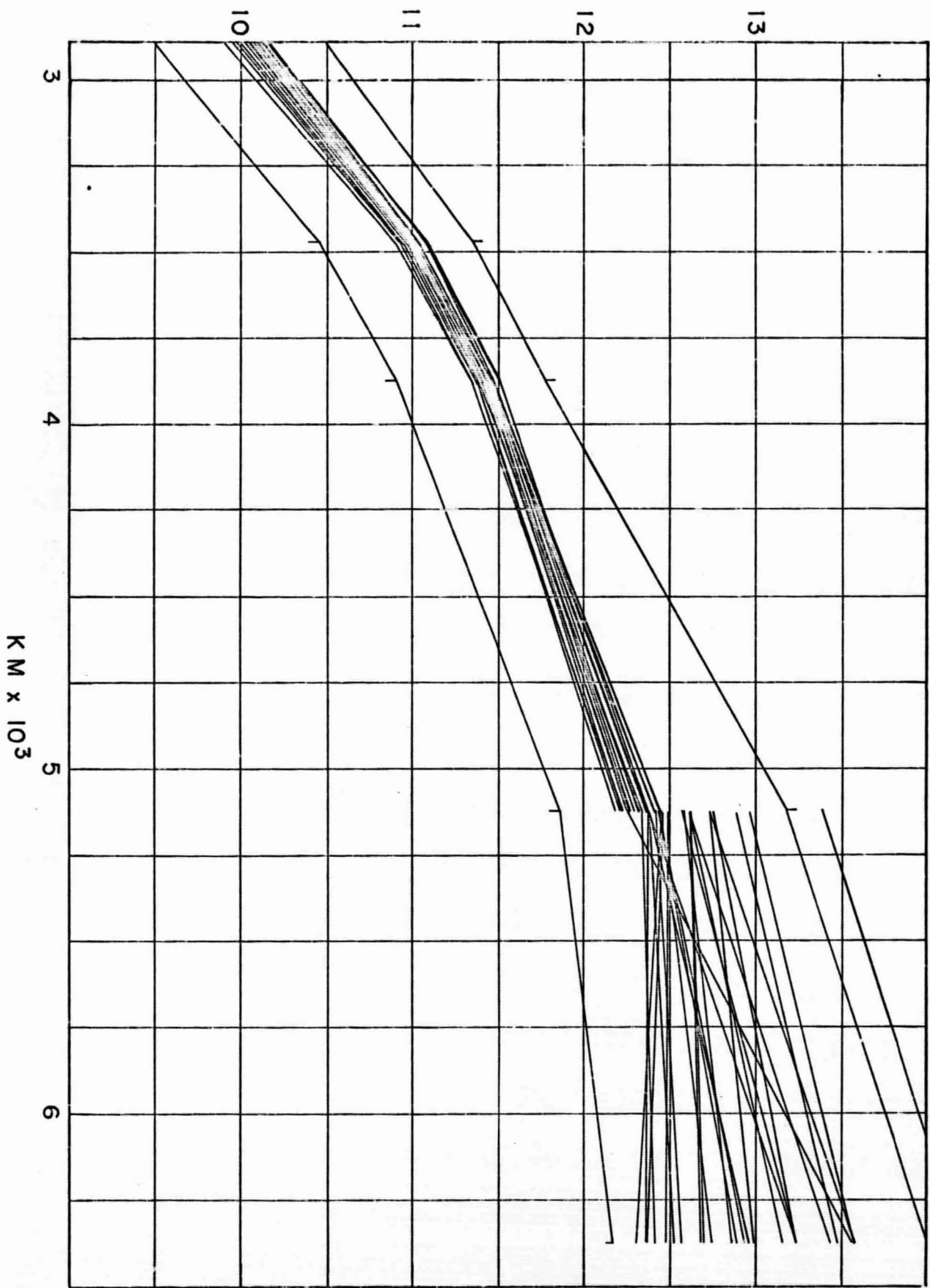
4.

5.

6.



GM / CC



DEPTH	ALPHA	RETA	RHO	ϕ	K/P	σ	10°	8.000	4.302	3.350	37.0	1.97	0.268	
7.0°	8.110	6.400	3.462	35.8	1.97	0.268	7.0°	8.000	4.302	3.350	37.0	1.97	0.268	
7.1°	9.110	6.470	3.550	39.7	1.97	0.268	7.1°	9.160	4.632	3.575	39.0	1.77	0.262	
7.2°	9.210	6.520	4.373	36.3	32.7	1.97	7.2°	9.267	4.760	4.204	35.6	1.03	0.270	
7.3°	9.310	6.580	4.268	3.370	47.7	2.64	0.332	7.3°	9.327	4.760	4.204	35.6	1.03	0.270
7.4°	9.410	6.630	4.201	3.257	45.5	2.16	0.280	7.4°	9.380	4.761	3.494	48.1	2.77	0.236
7.5°	9.510	6.680	4.034	3.460	44.2	1.99	0.275	7.5°	9.434	4.807	3.325	43.4	1.91	0.278
7.6°	9.610	6.730	3.491	3.491	40.4	1.33	0.312	7.6°	9.580	4.875	3.528	44.5	1.03	0.270
7.7°	9.710	6.780	3.755	4.168	56.2	1.71	0.255	7.7°	9.670	4.975	3.618	60.5	2.64	0.270
7.8°	9.810	6.830	5.734	4.414	76.7	2.14	0.209	7.8°	9.755	5.020	3.860	56.4	1.77	0.257
7.9°	9.910	6.880	5.993	4.414	76.7	1.91	0.277	7.9°	9.810	5.070	4.439	73.9	2.12	0.206
8.0°	10.010	6.930	6.222	4.406	74.0	1.91	0.277	8.0°	9.870	5.127	4.615	74.0	1.91	0.277
8.1°	10.110	6.980	6.575	4.793	86.8	2.01	0.294	8.1°	9.920	5.227	4.805	86.8	2.01	0.294
8.2°	10.210	7.030	7.040	5.117	103.7	2.01	0.294	8.2°	10.030	5.340	5.036	103.7	2.01	0.294
8.3°	10.310	7.080	7.346	6.263	117.7	2.14	0.301	8.3°	10.190	5.475	5.374	116.8	2.74	0.275
8.4°	10.410	7.130	7.690	7.202	120.3	2.14	0.301	8.4°	10.360	5.627	5.704	120.3	2.74	0.275
8.5°	10.510	7.180	8.010	8.600	11.464	0.0	0.0	8.5°	10.510	8.118	10.150	0.0	11.423	-----
8.6°	10.610	7.230	8.320	9.110	12.420	1.07	-----	8.6°	10.610	8.118	11.150	0.0	12.392	6.92
8.7°	10.710	7.280	8.630	9.613	13.420	1.07	-----	8.7°	10.710	8.371	11.150	0.0	13.523	-----
8.8°	10.810	7.330	9.110	10.110	14.420	1.07	-----	8.8°	10.810	8.574	11.150	0.0	14.552	-----
8.9°	10.910	7.380	9.613	10.603	15.420	1.07	-----	8.9°	10.910	8.774	11.150	0.0	15.681	-----
9.0°	11.010	7.430	10.110	11.110	16.420	1.07	-----	9.0°	11.010	8.974	11.150	0.0	16.810	-----
9.1°	11.110	7.480	10.603	11.603	17.420	1.07	-----	9.1°	11.110	9.174	11.150	0.0	17.939	-----
9.2°	11.210	7.530	11.110	12.110	18.420	1.07	-----	9.2°	11.210	9.374	11.150	0.0	19.068	-----
9.3°	11.310	7.580	11.603	12.603	19.420	1.07	-----	9.3°	11.310	9.574	11.150	0.0	20.197	-----
9.4°	11.410	7.630	12.110	13.110	20.420	1.07	-----	9.4°	11.410	9.774	11.150	0.0	21.326	-----
9.5°	11.510	7.680	12.603	13.603	21.420	1.07	-----	9.5°	11.510	9.974	11.150	0.0	22.455	-----
9.6°	11.610	7.730	13.110	14.110	22.420	1.07	-----	9.6°	11.610	10.174	11.150	0.0	23.584	-----
9.7°	11.710	7.780	13.603	14.603	23.420	1.07	-----	9.7°	11.710	10.374	11.150	0.0	24.713	-----
9.8°	11.810	7.830	14.110	15.110	24.420	1.07	-----	9.8°	11.810	10.574	11.150	0.0	25.842	-----
9.9°	11.910	7.880	14.603	15.603	25.420	1.07	-----	9.9°	11.910	10.774	11.150	0.0	26.971	-----
10.0°	12.010	7.930	15.110	16.110	26.420	1.07	-----	10.0°	12.010	10.974	11.150	0.0	28.100	-----
10.1°	12.110	7.980	15.603	16.603	27.420	1.07	-----	10.1°	12.110	11.174	11.150	0.0	29.229	-----
10.2°	12.210	8.030	16.110	17.110	28.420	1.07	-----	10.2°	12.210	11.374	11.150	0.0	30.358	-----
10.3°	12.310	8.080	16.603	18.110	29.420	1.07	-----	10.3°	12.310	11.574	11.150	0.0	31.487	-----
10.4°	12.410	8.130	17.110	18.603	30.420	1.07	-----	10.4°	12.410	11.774	11.150	0.0	32.616	-----
10.5°	12.510	8.180	17.603	19.110	31.420	1.07	-----	10.5°	12.510	11.974	11.150	0.0	33.745	-----
10.6°	12.610	8.230	18.110	19.603	32.420	1.07	-----	10.6°	12.610	12.174	11.150	0.0	34.874	-----
10.7°	12.710	8.280	18.603	20.110	33.420	1.07	-----	10.7°	12.710	12.374	11.150	0.0	35.003	-----
10.8°	12.810	8.330	19.110	20.603	34.420	1.07	-----	10.8°	12.810	12.574	11.150	0.0	36.132	-----
10.9°	12.910	8.380	19.603	21.110	35.420	1.07	-----	10.9°	12.910	12.774	11.150	0.0	37.261	-----
11.0°	13.010	8.430	20.110	21.603	36.420	1.07	-----	11.0°	13.010	12.974	11.150	0.0	38.390	-----
11.1°	13.110	8.480	20.603	22.110	37.420	1.07	-----	11.1°	13.110	13.174	11.150	0.0	39.519	-----
11.2°	13.210	8.530	21.110	22.603	38.420	1.07	-----	11.2°	13.210	13.374	11.150	0.0	40.648	-----
11.3°	13.310	8.580	21.603	23.110	39.420	1.07	-----	11.3°	13.310	13.574	11.150	0.0	41.777	-----
11.4°	13.410	8.630	22.110	23.603	40.420	1.07	-----	11.4°	13.410	13.774	11.150	0.0	42.906	-----
11.5°	13.510	8.680	22.603	24.110	41.420	1.07	-----	11.5°	13.510	13.974	11.150	0.0	44.035	-----
11.6°	13.610	8.730	23.110	24.603	42.420	1.07	-----	11.6°	13.610	14.174	11.150	0.0	45.164	-----
11.7°	13.710	8.780	23.603	25.110	43.420	1.07	-----	11.7°	13.710	14.374	11.150	0.0	46.293	-----
11.8°	13.810	8.830	24.110	25.603	44.420	1.07	-----	11.8°	13.810	14.574	11.150	0.0	47.422	-----
11.9°	13.910	8.880	24.603	26.110	45.420	1.07	-----	11.9°	13.910	14.774	11.150	0.0	48.551	-----
12.0°	14.010	8.930	25.110	26.603	46.420	1.07	-----	12.0°	14.010	14.974	11.150	0.0	49.680	-----
12.1°	14.110	8.980	25.603	27.110	47.420	1.07	-----	12.1°	14.110	15.174	11.150	0.0	50.809	-----
12.2°	14.210	9.030	26.110	27.603	48.420	1.07	-----	12.2°	14.210	15.374	11.150	0.0	51.938	-----
12.3°	14.310	9.080	26.603	28.110	49.420	1.07	-----	12.3°	14.310	15.574	11.150	0.0	53.067	-----
12.4°	14.410	9.130	27.110	28.603	50.420	1.07	-----	12.4°	14.410	15.774	11.150	0.0	54.196	-----
12.5°	14.510	9.180	27.603	29.110	51.420	1.07	-----	12.5°	14.510	15.974	11.150	0.0	55.325	-----
12.6°	14.610	9.230	28.110	29.603	52.420	1.07	-----	12.6°	14.610	16.174	11.150	0.0	56.454	-----
12.7°	14.710	9.280	28.603	29.110	53.420	1.07	-----	12.7°	14.710	16.374	11.150	0.0	57.583	-----
12.8°	14.810	9.330	29.110	29.603	54.420	1.07	-----	12.8°	14.810	16.574	11.150	0.0	58.712	-----
12.9°	14.910	9.380	29.603	29.110	55.420	1.07	-----	12.9°	14.910	16.774	11.150	0.0	59.841	-----
13.0°	15.010	9.430	30.110	29.603	56.420	1.07	-----	13.0°	15.010	16.974	11.150	0.0	60.970	-----
13.1°	15.110	9.480	30.603	29.110	57.420	1.07	-----	13.1°	15.110	17.174	11.150	0.0	62.109	-----
13.2°	15.210	9.530	31.110	29.603	58.420	1.07	-----	13.2°	15.210	17.374	11.150	0.0	63.238	-----
13.3°	15.310	9.580	31.603	29.110	59.420	1.07	-----	13.3°	15.310	17.574	11.150	0.0	64.367	-----
13.4°	15.410	9.630	32.110	29.603	60.420	1.07	-----	13.4°	15.410	17.774	11.150	0.0	65.506	-----
13.5°	15.510	9.680	32.603	29.110	61.420	1.07	-----	13.5°	15.510	17.974	11.150	0.0	66.635	-----
13.6°	15.610	9.730	33.110	29.603	62.420	1.07	-----	13.6°	15.610	18.174	11.150	0.0	67.764	-----
13.7°	15.710	9.780	33.603	29.110	63.420	1.07	-----	13.7°	15.710	18.374	11.150	0.0	68.893	-----
13.8°	15.810	9.830	34.110	29.603	64.420	1.07	-----	13.8°	15.810	18.574	11.150	0.0	70.022	-----
13.9°	15.910	9.880	34.603	29.110	65.420	1.07	-----	13.9°	15.910	18.774	11.150	0.0	71.151	-----
14.0°	16.010	9.930	35.110	29.603	66.420	1.07	-----	14.0°	16.010	18.974	11.150	0.0	72.280	-----
14.1°	16.110	9.980	35.603	29.110	67.420	1.07	-----	14.1°	16.110	19.174	11.150	0.0	73.409	-----
14.2°	16.210	10.030	36.110	29.603	68.420	1.07	-----	14.2°	16.210	19.374	11.150	0.0	74.538	-----
14.3°	16.310	10.080	36.603	29.110	69.420	1.07	-----	14.3°	16.310	19.574	11.150	0.0	75.667	-----
14.4°	16.410	10.130	37.110	29.603	70.420	1.07	-----	14.4°	16.410	19.774	11.150	0.0	76.796	-----
14.5°	16.510	10.180	37.603	29.110	71.420	1.07	-----	14.5°	16.510</td					

n	10.	8.000	4.033	3.045	36.0	1.70	8.000	4.400	3.271	37.1	1.84	8.020					
n	71.	8.160	4.585	3.501	38.6	1.83	8.260	71.	9.160	4.585	3.572	38.6	1.93	8.260			
n	146.	7.760	4.039	3.550	34.0	1.77	8.260	7.760	4.451	3.533	33.8	1.71	8.265				
n	221.	8.470	4.224	3.550	48.0	2.60	8.334	221.	9.470	4.200	3.498	49.1	2.72	8.336			
n	296.	8.580	4.202	3.503	40.1	2.65	8.333	296.	9.580	4.417	3.504	47.7	2.45	8.336			
n	371.	8.680	4.889	3.681	43.5	1.82	8.260	371.	9.680	4.947	3.388	44.0	1.97	9.273			
n	451.	8.678	5.230	3.500	57.0	2.06	8.263	451.	9.678	5.122	3.502	58.2	2.73	0.385			
n	621.	10.000	5.680	3.819	56.9	1.76	8.261	621.	10.000	5.673	4.016	57.1	1.77	8.263			
n	771.	10.070	5.965	4.256	72.9	2.05	8.260	771.	10.070	5.936	4.446	73.5	2.05	8.264			
n	871.	11.210	6.265	4.661	73.3	1.87	8.273	871.	11.210	6.207	4.548	74.3	1.93	8.273			
n	1271.	17.020	6.571	6.962	96.0	2.61	8.267	1271.	17.020	6.589	6.767	86.6	1.95	8.273			
n	2171.	13.030	7.057	5.116	103.4	2.08	8.262	2171.	13.030	7.078	5.053	103.0	2.05	8.265			
n	2809.	13.770	7.277	5.272	119.0	2.25	8.260	2809.	13.770	7.270	5.390	119.1	2.25	8.267			
n	3461.	9.000	0.0	10.945	10.945	0.0	8.260	3461.	9.000	0.0	10.947	10.947	0.0	8.264			
n	3871.	0.600	0.0	11.399	11.399	0.0	8.260	3871.	0.600	0.0	11.399	11.399	0.0	8.264			
n	5119.	10.150	7.07	12.749	6.42	-----	5119.	10.150	7.07	12.745	6.21	-----	5119.	10.150	7.07	12.745	
n	6371.	11.100	0.0	13.271	13.271	0.0	8.260	6371.	11.100	0.0	13.271	13.271	0.0	8.264			
n	10.	8.000	4.0487	3.281	37.2	1.85	8.071	10.	8.000	4.520	3.354	36.7	1.70	8.064			
n	71.	8.160	4.645	3.597	37.5	1.75	8.260	71.	8.160	4.520	3.571	39.3	1.93	8.270			
n	146.	7.760	4.268	3.632	36.6	1.98	8.264	146.	7.760	4.308	3.525	35.5	1.91	8.274			
n	221.	8.470	4.313	3.674	46.9	2.52	8.315	221.	9.470	4.630	3.533	45.5	2.31	8.311			
n	296.	8.580	4.445	3.365	47.3	2.36	8.317	296.	8.580	4.404	3.406	46.7	2.31	8.311			
n	371.	8.680	4.801	3.157	42.4	1.81	8.267	371.	8.680	4.698	3.209	45.9	2.08	8.273			
n	451.	8.678	5.200	3.476	56.2	2.01	8.266	451.	9.678	5.229	3.296	57.1	2.00	8.273			
n	621.	10.000	5.550	3.953	59.9	1.91	8.277	621.	10.000	5.661	3.980	57.6	1.91	8.277			
n	771.	10.570	5.926	6.384	73.0	2.05	8.261	771.	10.570	5.874	6.561	74.3	2.15	8.266			
n	871.	11.210	6.201	4.544	74.4	1.93	8.280	871.	11.210	6.212	4.640	74.2	1.92	8.279			
n	1271.	17.020	6.571	6.960	9.01	0.98	8.267	1271.	17.020	6.581	6.932	87.4	2.04	8.266			
n	2171.	13.030	7.051	5.103	103.5	2.09	8.263	2171.	13.030	7.052	5.089	103.5	2.08	8.263			
n	2809.	13.770	7.362	5.264	117.3	2.17	8.260	2809.	13.770	7.336	5.324	117.0	2.17	8.262			
n	3461.	7.060	0.0	10.115	10.115	0.0	8.260	3461.	7.060	0.0	10.027	10.027	0.0	8.264			
n	3871.	6.700	0.0	11.028	11.028	0.0	8.260	3871.	6.700	0.0	11.361	11.361	0.0	8.264			
n	5119.	10.150	0.0	12.711	3.38	-----	5119.	10.150	0.0	12.726	5.04	-----	5119.	10.150	0.0	12.726	
n	6371.	11.100	0.0	13.253	13.253	0.0	8.260	6371.	11.100	0.0	12.096	-----	6371.	11.100	0.0	12.096	
n	10.	8.000	4.0560	3.298	36.3	1.74	8.050	10.	8.000	4.683	3.321	34.8	1.58	8.030			
n	71.	8.160	4.533	3.619	39.7	1.71	8.277	71.	9.160	4.504	3.400	30.5	1.05	8.281			
n	146.	7.760	4.427	3.609	36.1	1.76	8.260	146.	7.760	4.274	3.590	36.1	1.74	8.260			
n	221.	8.470	4.247	3.609	47.7	2.64	8.317	221.	9.470	4.255	3.551	47.5	2.61	8.319			
n	296.	8.580	4.520	3.318	46.6	2.27	8.309	296.	8.580	4.326	3.436	48.7	2.60	8.310			
n	371.	8.680	4.781	3.366	44.0	1.96	8.282	371.	8.680	4.931	3.467	44.2	1.80	8.276			
n	451.	8.678	5.226	3.553	57.1	2.09	8.266	451.	9.678	5.223	3.303	57.1	2.00	8.266			
n	621.	10.000	5.541	4.195	50.1	1.92	8.278	621.	10.000	5.550	4.117	50.0	1.91	8.277			
n	771.	10.570	5.951	4.403	73.1	2.06	8.261	771.	10.570	5.914	4.570	73.7	2.11	8.265			
n	871.	11.210	6.256	4.721	73.5	1.88	8.274	871.	11.210	6.206	4.626	74.3	1.91	8.276			
n	1271.	17.020	6.598	4.726	86.6	2.00	8.285	1271.	17.020	6.570	4.812	86.0	2.01	8.287			
n	2171.	13.030	7.037	5.119	103.9	2.10	8.254	2171.	13.030	7.106	4.973	102.5	2.03	8.288			
n	2809.	13.770	7.307	5.204	110.4	2.27	8.264	2809.	13.770	7.311	5.370	110.3	2.11	8.266			
n	3471.	9.000	0.0	11.088	11.088	0.0	8.260	3471.	9.000	0.0	10.976	10.976	0.0	8.264			
n	3871.	9.600	0.0	11.505	11.505	0.0	8.260	3871.	9.600	0.0	11.437	11.437	0.0	8.264			
n	5119.	10.150	0.0	12.336	-2.37	-----	5119.	10.150	0.0	12.446	4.03	-----	5119.	10.150	0.0	12.446	
n	6371.	11.100	0.0	13.169	13.169	0.0	8.260	6371.	11.100	0.0	13.202	4.03	-----	6371.	11.100	0.0	13.202

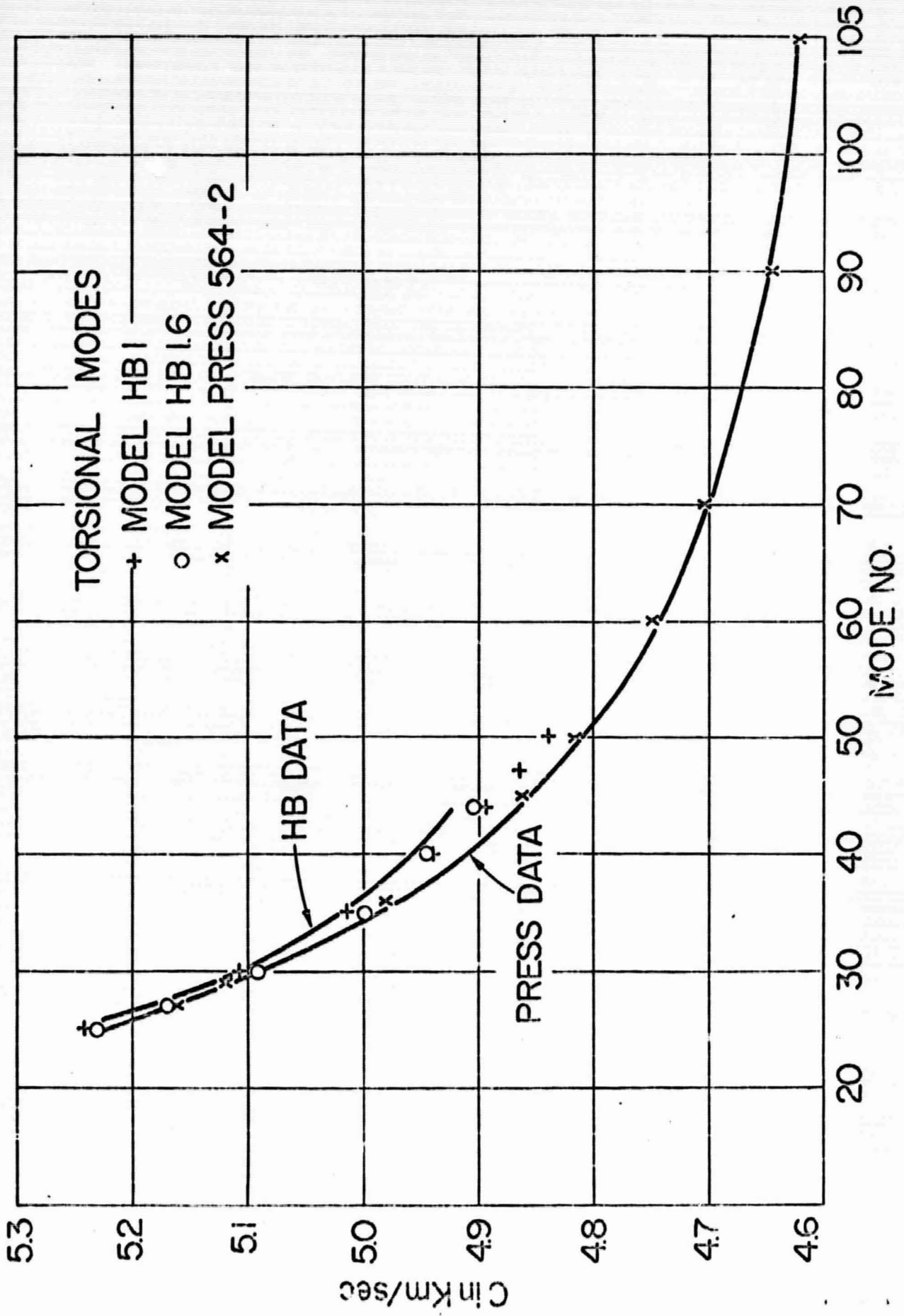
n	16.	8.000	4.623	3.436	25.6	1.66	0.249	10.	8.000	4.628	3.394	35.6	1.66	0.245	
n	71.	8.160	4.609	3.512	39.6	1.06	0.282	71.	8.160	4.606	3.509	30.8	1.06	0.282	
n	165.	7.660	4.613	3.619	34.9	1.83	0.269	165.	7.660	4.631	3.555	36.6	1.83	0.269	
n	721.	8.470	4.583	3.532	46.6	2.47	0.322	721.	8.470	4.583	3.259	46.4	2.44	0.310	
n	796.	8.590	4.673	3.585	47.9	2.66	0.321	796.	8.580	4.628	3.278	46.7	2.67	0.303	
n	371.	8.680	4.712	3.525	45.7	2.06	0.291	371.	8.680	4.696	3.572	45.0	2.09	0.293	
n	471.	8.670	5.317	3.395	55.0	1.98	0.294	471.	8.670	5.157	3.654	58.0	2.04	0.291	
n	621.	10.000	5.561	4.110	58.8	1.90	0.276	621.	10.000	5.445	4.026	60.5	2.04	0.289	
n	721.	10.970	5.670	4.473	72.7	2.03	0.280	721.	10.970	5.347	4.337	73.3	2.07	0.292	
n	871.	11.210	6.232	4.569	73.0	1.90	0.276	871.	11.210	6.236	4.464	73.8	1.90	0.274	
n	13.71.	12.490	6.673	4.917	86.9	2.01	0.267	13.71.	12.470	6.590	4.803	86.8	1.96	0.265	
n	271.	13.030	7.056	5.029	103.4	2.09	0.201	271.	13.030	7.042	5.104	103.7	2.09	0.204	
n	289.	13.770	7.792	5.378	118.7	2.03	0.202	289.	13.770	7.316	5.271	117.0	2.04	0.207	
n	289.	7.960	8.000	10.075	289.	7.960	8.000	10.075	289.	7.960	8.000	10.075	289.	7.960	8.000
n	3471.	9.000	8.000	8.000	3471.	9.000	8.000	8.000	3471.	9.000	8.000	8.000	3471.	9.000	8.000
n	1871.	9.600	8.000	11.453	3471.	9.600	8.000	11.453	3471.	9.600	8.000	11.453	3471.	9.600	8.000
n	2118.	10.150	8.000	12.352	3.75	-----	-----	2118.	10.150	8.000	12.352	3.75	-----	-----	
n	5118.	11.150	8.000	12.882	-----	-----	-----	5118.	11.150	8.000	12.882	-----	-----	-----	
n	6371.	11.160	8.000	13.477	6371.	11.160	8.000	13.477	6371.	11.160	8.000	13.477	6371.	11.160	8.000
n	170.	8.000	4.506	3.395	36.0	1.82	0.268	170.	8.000	4.522	3.395	36.7	1.90	0.266	
n	71.	8.160	4.560	3.410	37.5	1.72	0.257	71.	8.160	4.594	3.505	38.4	1.82	0.268	
n	146.	7.760	4.351	3.577	35.0	1.84	0.276	146.	7.760	4.275	3.519	36.6	1.84	0.286	
n	721.	8.420	4.313	3.564	46.9	2.52	0.326	721.	8.420	4.231	3.520	47.0	2.47	0.314	
n	796.	8.580	4.625	3.645	49.5	2.74	0.327	796.	8.580	4.725	3.617	49.5	2.67	0.305	
n	371.	8.650	4.673	3.703	45.2	2.11	0.295	371.	8.650	4.894	3.761	43.6	1.83	0.295	
n	471.	8.650	5.260	4.170	56.1	1.71	0.255	471.	8.650	5.246	3.547	56.8	2.04	0.281	
n	621.	10.000	5.735	4.315	74.6	1.94	0.280	621.	10.000	5.430	3.919	60.7	2.06	0.291	
n	721.	10.970	6.095	4.315	74.6	1.94	0.280	721.	10.970	6.087	4.577	74.1	2.04	0.286	
n	871.	11.210	6.107	4.647	74.5	1.94	0.280	871.	11.210	6.266	4.614	73.3	1.97	0.272	
n	1771.	12.020	6.585	4.772	86.7	2.06	0.286	1771.	12.020	6.585	4.637	86.5	2.06	0.286	
n	2171.	13.030	7.067	5.102	103.2	2.07	0.202	2171.	13.030	7.050	5.071	103.5	2.09	0.202	
n	2908.	13.770	7.271	5.365	119.1	2.26	0.307	2908.	13.770	7.350	5.296	117.6	2.19	0.301	
n	289.	7.960	8.000	10.075	289.	7.960	8.000	10.075	289.	7.960	8.000	10.075	289.	7.960	8.000
n	3471.	9.000	8.000	11.392	3471.	9.000	8.000	11.392	3471.	9.000	8.000	11.392	3471.	9.000	8.000
n	1871.	9.600	8.000	11.392	3471.	9.600	8.000	11.392	3471.	9.600	8.000	11.392	3471.	9.600	8.000
n	5119.	10.150	8.000	12.352	3.77	-----	-----	5119.	10.150	8.000	12.352	3.77	-----	-----	
n	6371.	11.160	8.000	13.477	6371.	11.160	8.000	13.477	6371.	11.160	8.000	13.477	6371.	11.160	8.000
n	170.	8.000	4.610	3.420	35.7	1.68	0.261	170.	8.000	4.630	3.213	35.3	1.64	0.247	
n	71.	8.160	4.501	3.482	30.6	1.95	0.281	71.	8.160	4.503	3.504	39.5	1.97	0.284	
n	146.	7.760	4.595	3.563	36.4	2.04	0.280	146.	7.760	4.276	3.501	36.8	2.04	0.286	
n	2171.	8.470	4.513	3.567	44.6	2.10	0.302	2171.	8.470	4.270	3.500	47.0	2.08	0.304	
n	796.	8.580	4.553	3.515	45.0	2.70	0.302	796.	8.580	4.717	3.337	42.0	1.99	0.293	
n	371.	8.650	4.643	3.501	46.6	2.01	0.300	371.	8.650	4.955	3.291	42.0	1.96	0.277	
n	471.	8.650	5.260	3.506	50.8	2.37	0.315	471.	8.650	5.141	3.503	46.3	2.09	0.303	
n	621.	10.000	5.672	4.122	57.1	1.77	0.263	621.	10.000	5.450	3.977	60.3	2.03	0.280	
n	721.	10.970	5.672	4.195	73.1	1.95	0.261	721.	10.970	5.674	4.73.3	72.0	1.99	0.263	
n	871.	11.210	6.040	4.552	73.6	1.89	0.276	871.	11.210	6.016	4.611	73.0	1.90	0.274	
n	1771.	12.020	6.575	4.377	96.9	2.01	0.287	1771.	12.020	6.595	4.908	96.7	2.00	0.285	
n	2171.	13.030	7.036	5.003	103.9	2.10	0.204	2171.	13.030	7.020	5.024	104.1	2.11	0.206	
n	2908.	13.770	7.155	5.205	117.5	2.17	0.300	2908.	13.770	7.366	5.236	117.5	2.17	0.300	
n	289.	7.960	8.000	10.075	289.	7.960	8.000	10.075	289.	7.960	8.000	10.075	289.	7.960	8.000
n	3471.	9.000	8.000	10.075	3471.	9.000	8.000	10.075	3471.	9.000	8.000	10.075	3471.	9.000	8.000
n	1871.	9.600	8.000	11.392	3471.	9.600	8.000	11.392	3471.	9.600	8.000	11.392	3471.	9.600	8.000
n	5119.	10.150	8.000	12.352	9.82	-----	-----	5119.	10.150	8.000	12.352	9.82	-----	-----	
n	6371.	11.160	8.000	13.477	6371.	11.160	8.000	13.477	6371.	11.160	8.000	13.477	6371.	11.160	8.000

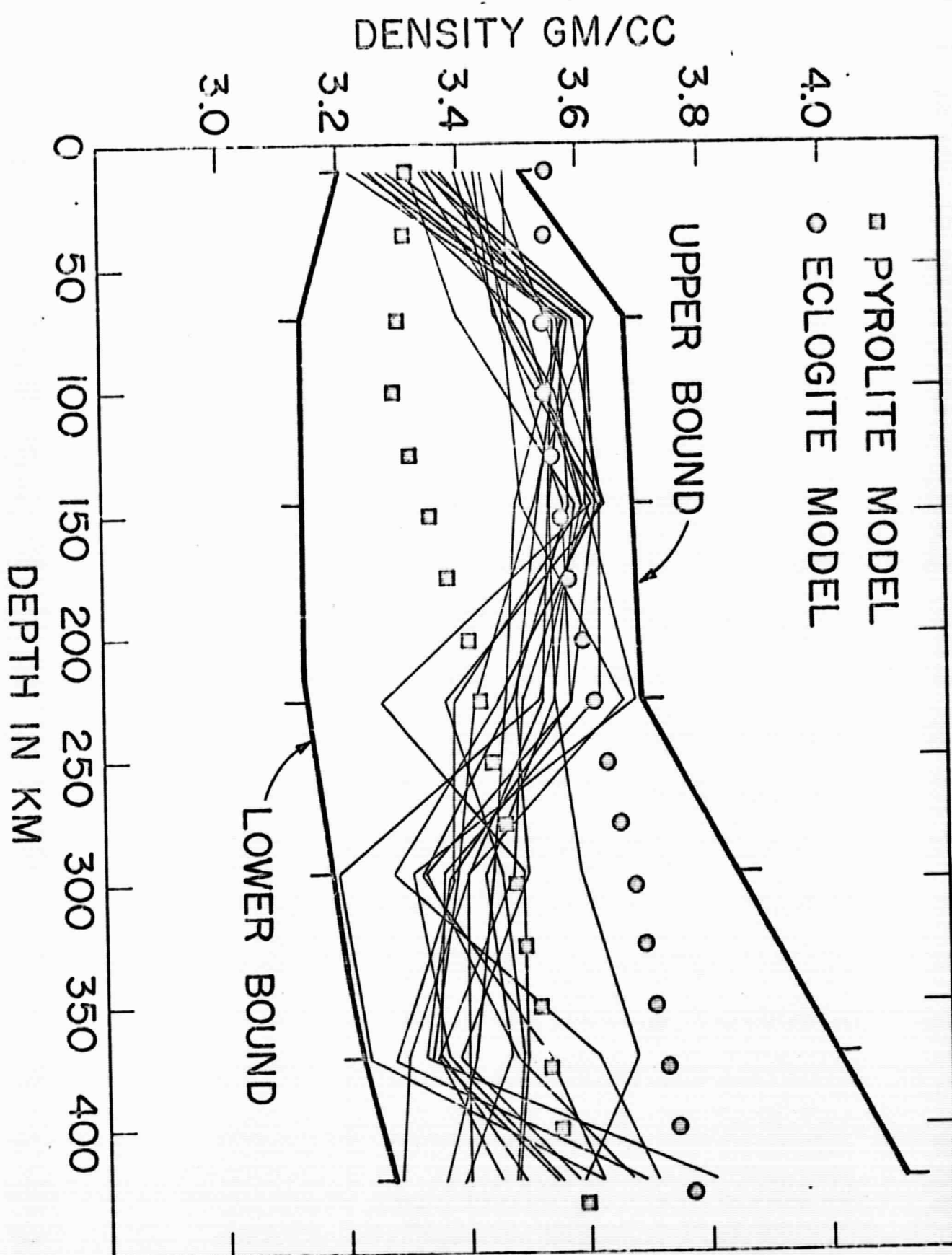
79.	9.000	6.576	3.617	36.1	1.77	0.267	10.	9.000	4.030	3.992	36.6	1.76	0.264
71.	9.160	4.574	3.601	10.7	1.91	0.277	71.	9.160	4.400	3.575	39.6	1.96	0.282
166.	7.760	6.311	3.621	35.4	1.91	0.277	146.	7.760	4.363	3.605	35.1	1.96	0.279
221.	9.470	6.376	3.263	46.7	2.41	0.318	221.	9.470	4.350	3.477	46.5	2.46	0.321
760.	9.580	6.556	3.876	45.9	2.71	0.304	776.	8.580	4.503	3.665	45.4	2.75	0.305
371.	9.680	4.571	3.503	48.1	2.34	0.313	371.	9.680	4.620	3.619	46.9	2.39	0.302
471.	9.670	6.208	3.278	57.3	2.11	0.286	471.	9.670	6.070	3.355	56.2	2.19	0.316
621.	10.000	5.672	4.145	57.9	1.93	0.269	621.	10.000	5.701	6.220	56.7	1.94	0.265
721.	10.970	5.860	4.332	74.6	2.17	0.300	721.	10.970	5.914	6.415	73.7	2.11	0.295
871.	11.210	6.263	4.688	73.4	1.87	0.273	871.	11.210	6.258	4.605	73.4	1.88	0.274
1371.	12.020	6.607	4.860	96.5	1.99	0.284	1371.	12.020	6.521	4.775	87.8	2.06	0.291
2171.	13.030	7.020	5.107	103.9	2.10	0.295	2171.	13.030	7.085	5.008	102.9	2.05	0.290
2698.	13.770	7.376	5.766	117.1	2.15	0.299	2698.	13.770	7.340	5.703	117.8	2.16	0.302
2898.	7.960	0.000	0.0	10.056	—	—	2898.	7.960	0.0	0.031	10.031	—	—
3471.	9.600	0.0	11.370	—	—	—	3471.	9.600	0.0	10.965	10.965	—	—
3871.	10.150	0.0	12.733	5.70	—	—	3871.	10.150	0.0	12.375	7.43	—	—
5118.	11.190	0.0	13.877	—	—	—	5118.	11.190	0.0	13.236	—	—	—
6371.	11.190	0.0	13.877	—	—	—	6371.	11.190	0.0	13.236	—	—	—
16.	9.000	4.587	3.432	35.9	1.71	0.255	10.	8.000	4.573	3.345	36.1	1.73	0.257
71.	9.160	4.504	3.466	30.5	1.95	0.281	71.	9.160	4.540	3.611	39.1	1.90	0.276
146.	7.760	6.338	3.670	45.1	1.67	0.273	146.	7.760	4.298	3.617	35.7	1.65	0.281
221.	9.470	6.345	3.579	46.6	2.47	0.321	221.	9.470	4.243	3.503	47.7	2.65	0.332
266.	9.580	6.522	3.366	46.4	2.27	0.308	266.	8.580	4.733	3.678	43.7	1.65	0.281
371.	9.680	4.693	3.335	46.1	2.10	0.295	371.	9.680	4.822	3.348	44.3	1.91	0.277
471.	9.670	6.589	3.522	50.0	2.08	0.300	471.	9.670	5.081	3.640	59.1	2.20	0.300
621.	10.000	5.659	4.002	55.8	1.69	0.252	621.	10.000	5.694	4.012	56.8	1.75	0.260
721.	10.970	6.051	4.366	73.1	2.05	0.291	721.	10.970	5.921	6.435	73.6	2.05	0.284
871.	11.210	6.231	4.487	73.9	1.90	0.276	871.	11.210	6.195	4.563	74.5	1.94	0.280
1371.	12.020	6.560	4.662	87.1	2.03	0.288	1371.	12.020	6.600	4.802	86.4	1.98	0.288
2171.	13.030	7.057	5.564	103.5	2.09	0.293	2171.	13.030	7.005	5.047	104.4	2.13	0.297
2698.	13.770	7.371	5.262	117.2	2.16	0.299	2698.	13.770	7.373	5.398	117.1	2.15	0.299
2898.	7.960	0.0	10.150	—	—	—	2898.	7.960	0.0	10.087	10.087	—	—
3471.	9.600	0.0	11.370	—	—	—	3471.	9.600	0.0	11.002	11.002	—	—
3871.	10.150	0.0	12.710	6.17	—	—	3871.	10.150	0.0	12.424	12.424	—	—
5118.	11.150	0.0	12.450	—	—	—	5118.	11.150	0.0	12.443	1.64	—	—
6371.	11.190	0.0	12.361	—	—	—	6371.	11.190	0.0	12.877	—	—	—
16.	9.000	4.619	3.727	36.8	1.80	0.266	10.	9.000	4.625	3.437	35.3	1.66	0.263
71.	9.160	4.612	3.514	38.2	1.80	0.265	71.	9.160	4.647	3.466	37.9	1.75	0.260
146.	7.760	4.716	3.614	36.5	2.05	0.201	146.	7.760	4.101	3.567	36.8	2.05	0.204
221.	9.470	6.301	3.512	47.1	2.54	0.226	221.	8.470	4.384	3.578	46.1	2.40	0.217
266.	9.580	4.656	3.180	44.7	2.06	0.291	266.	8.580	4.424	3.342	47.5	2.63	0.210
371.	9.680	4.689	3.217	44.0	2.09	0.294	371.	9.680	4.680	4.747	43.8	1.96	0.272
471.	9.670	5.305	3.610	56.0	1.90	0.285	471.	9.670	5.281	3.671	55.3	2.05	0.287
621.	10.000	5.667	4.014	60.1	2.01	0.287	621.	10.000	5.416	3.866	60.9	2.09	0.292
721.	10.970	5.940	4.307	74.7	2.18	0.281	721.	10.970	5.958	4.465	73.0	2.06	0.291
871.	11.210	6.235	4.555	73.9	1.90	0.276	871.	11.210	6.212	4.571	74.2	1.97	0.278
1371.	12.020	6.500	4.666	86.6	1.90	0.285	1371.	12.020	6.549	4.702	87.3	2.04	0.280
2171.	13.030	7.050	5.095	103.5	2.04	0.291	2171.	13.030	7.101	5.070	102.5	2.07	0.280
2698.	13.770	7.370	5.419	116.7	2.21	0.293	2698.	13.770	7.340	5.293	117.6	2.19	0.301
2898.	7.960	0.0	9.070	—	—	—	2898.	7.960	0.0	10.075	10.075	—	—
3471.	9.600	0.0	11.338	—	—	—	3471.	9.600	0.0	10.973	10.973	—	—
3871.	10.150	0.0	12.227	10.33	—	—	3871.	9.600	0.0	11.430	11.430	—	—
5118.	11.150	0.0	12.264	—	—	—	5118.	11.150	0.0	12.613	9.71	—	—
6371.	11.190	0.0	12.367	—	—	—	6371.	11.190	0.0	12.593	—	—	—

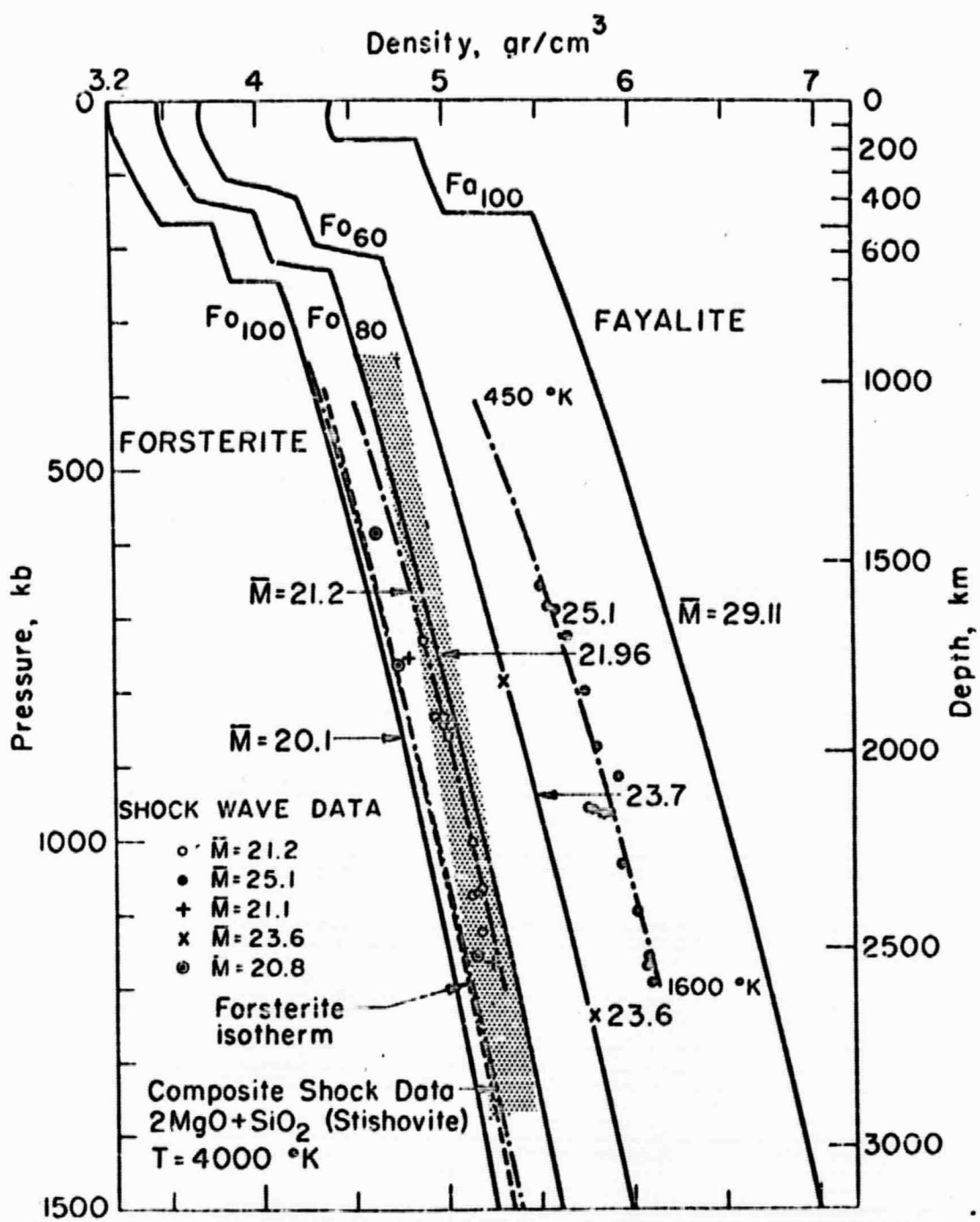
"	10.	8.000	4.610	3.333	35.7	1.69	0.251
"	71.	8.160	4.558	3.527	38.9	1.87	0.273
"	146.	7.760	4.428	3.559	34.1	1.74	0.259
"	221.	8.470	4.151	3.580	48.8	2.83	0.342
"	296.	8.580	4.594	3.323	45.5	2.15	0.299
"	371.	8.680	4.770	3.392	45.0	1.98	0.284
"	421.	9.670	5.050	3.762	59.5	2.33	0.312
"	621.	10.000	5.740	3.849	56.1	1.70	0.254
"	721.	10.970	5.930	4.471	73.5	2.09	0.294
"	871.	11.210	6.253	4.607	73.5	1.88	0.274
"	1371.	12.020	6.545	4.799	97.4	2.04	0.289
"	2171.	13.030	7.025	5.007	104.0	2.11	0.295
"	2898.	13.770	7.377	5.238	117.1	2.15	0.299
"	2898.	7.960	0.0	10.155			
"	3471.	9.000	0.0	11.076			
"	3871.	9.600	0.0	11.451			
"	5118.	10.150	0.0	12.373		-3.41	
"	5118.	11.150	0.0	12.493			
"	6371.	11.190	0.0	12.471			

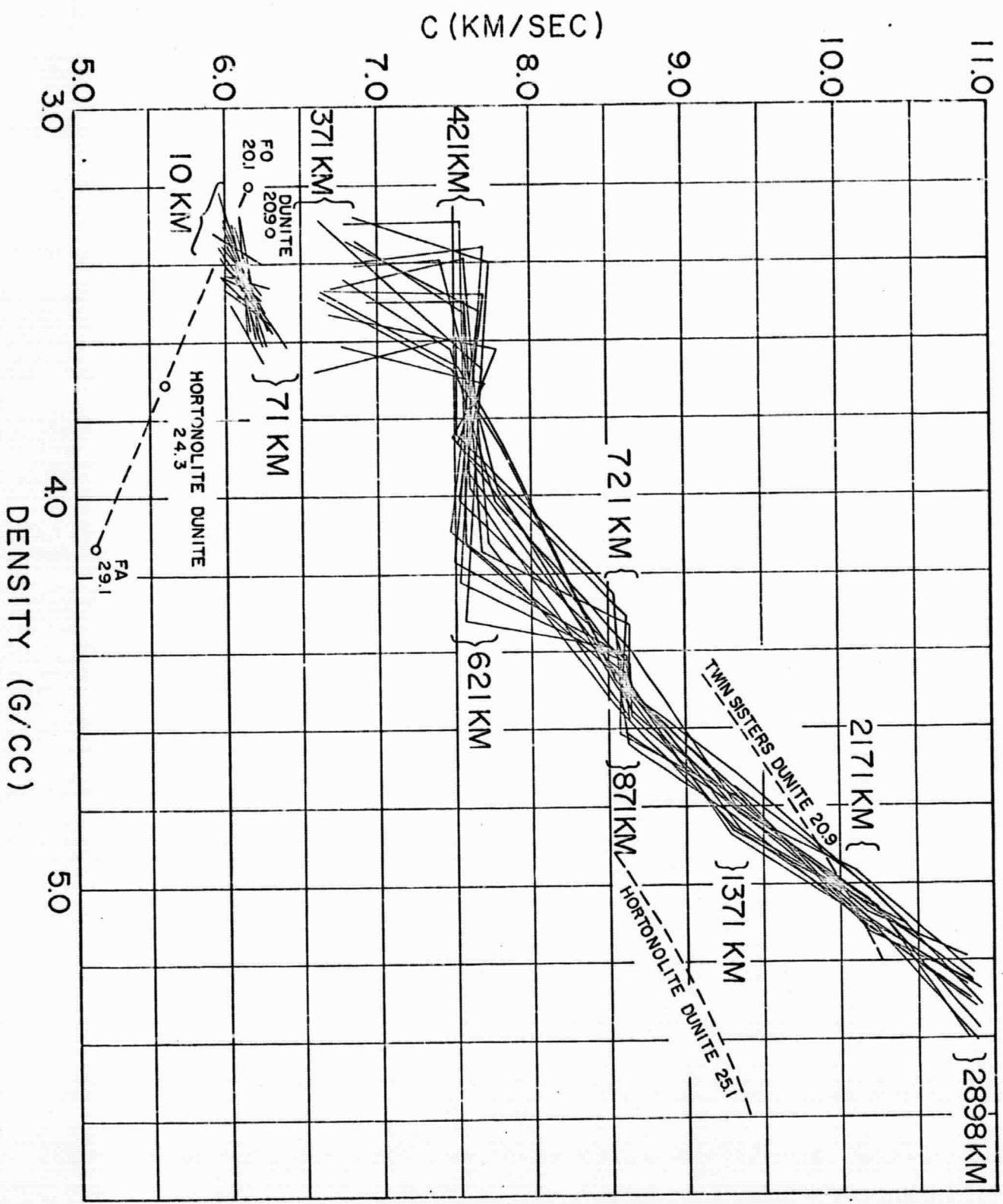
"	10.	8.000	4.552	3.514	36.4	1.76	0.261
"	71.	8.160	4.536	3.659	39.2	1.90	0.276
"	146.	7.760	4.332	3.598	35.2	1.88	0.274
"	221.	8.470	4.377	3.572	46.2	2.41	0.318
"	296.	8.580	4.413	3.373	47.7	2.45	0.320
"	371.	8.680	4.840	3.477	44.1	1.88	0.274
"	421.	9.670	5.318	3.684	55.8	1.97	0.283
"	621.	10.000	5.515	4.041	59.4	1.95	0.281
"	721.	10.970	5.933	4.308	73.4	2.09	0.293
"	871.	11.210	6.263	4.470	73.4	1.87	0.273
"	1371.	12.020	6.587	4.718	96.6	2.00	0.285
"	2171.	13.030	7.048	5.086	103.5	2.08	0.293
"	2898.	13.770	7.343	5.341	117.7	2.18	0.301
"	2898.	7.960	0.0	10.182			
"	3471.	9.000	0.0	11.076			
"	3871.	9.600	0.0	11.476			
"	5118.	10.150	0.0	12.261		3.33	
"	5118.	11.150	0.0	12.449			
"	6371.	11.190	0.0	12.300			

"	10.	8.000	4.601	3.289	35.8	1.69	0.253
"	71.	8.160	4.557	3.542	38.9	1.87	0.273
"	146.	7.760	4.316	3.513	35.4	1.90	0.276
"	221.	8.470	4.402	3.515	45.9	2.37	0.315
"	296.	8.580	4.451	3.583	47.2	2.38	0.316
"	371.	8.680	4.522	3.274	48.1	2.35	0.314
"	421.	9.670	5.252	3.686	56.7	2.06	0.291
"	621.	10.000	5.660	3.769	57.3	1.79	0.264
"	721.	10.970	5.891	4.484	74.1	2.13	0.297
"	871.	11.210	6.202	4.644	74.4	1.93	0.279
"	1371.	12.020	6.598	4.807	96.4	1.99	0.284
"	2171.	13.030	7.047	5.051	103.6	2.09	0.293
"	2898.	13.770	7.281	5.218	118.9	2.24	0.306
"	2898.	7.960	0.0	10.041			
"	3471.	9.000	0.0	10.996			
"	3871.	9.600	0.0	11.450			
"	5118.	10.150	0.0	12.426		4.28	
"	5118.	11.150	0.0	12.578			
"	6371.	11.190	0.0	12.853			

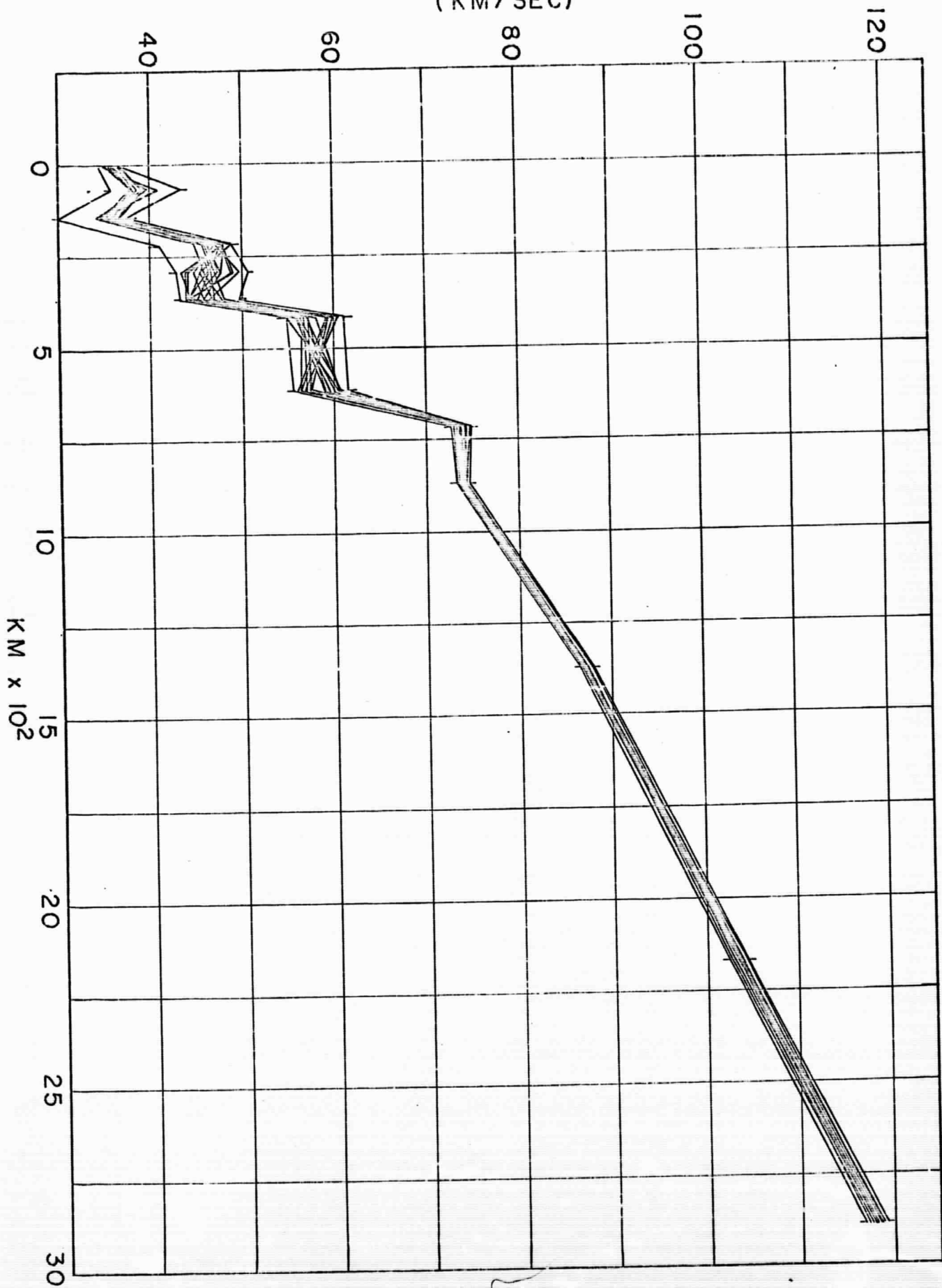


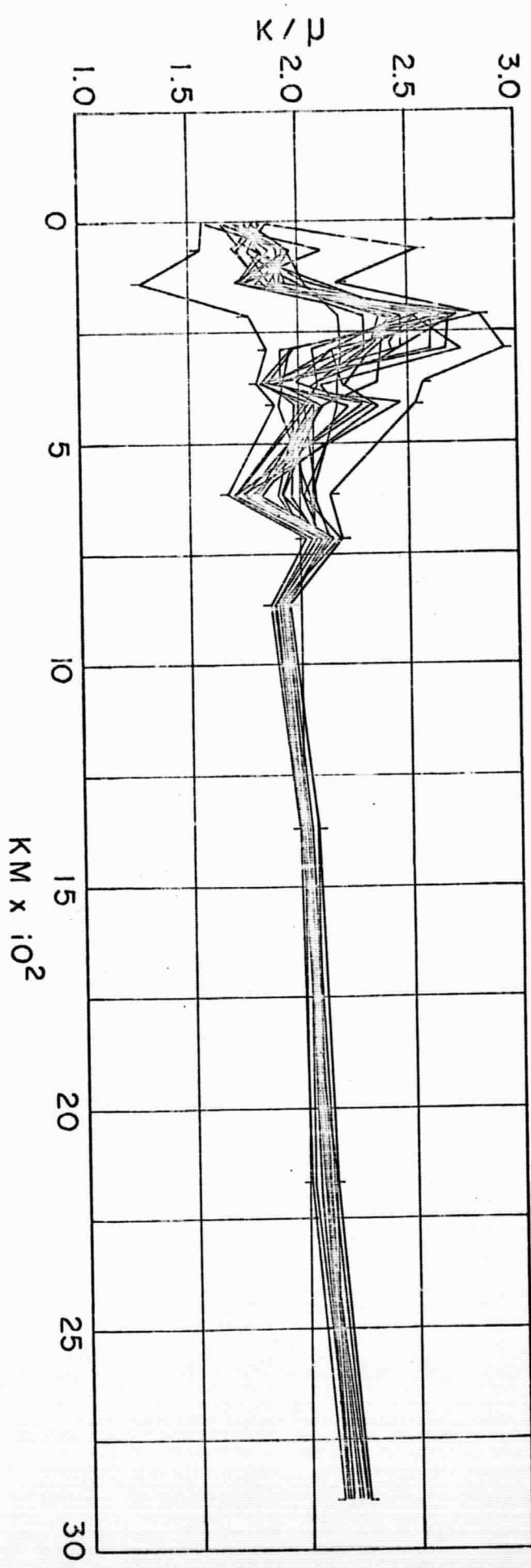






$(\text{KM/SEC})^2$





DENSITY G/CC

